

# Near-threshold $\omega$ and $\phi$ meson productions in $pp$ collisions

K. Tsushima<sup>1</sup>, and K. Nakayama<sup>1,2</sup>

<sup>1</sup>*Department of Physics and Astronomy, University of Georgia, Athens, Georgia 30602, USA*

<sup>2</sup>*Institut für Kernphysik, Forschungszentrum-Jülich, D-52425, Jülich, Germany*

## Abstract

Using a relativistic effective Lagrangian at the hadronic level, near-threshold  $\omega$  and  $\phi$  meson productions in proton proton ( $pp$ ) collisions,  $pp \rightarrow pp\omega/\phi$ , are studied within the distorted wave Born approximation. Both initial and final state  $pp$  interactions are included. In addition to total cross section data, both  $\omega$  and  $\phi$  angular distribution data are used to constrain further the model parameters. For the  $pp \rightarrow pp\omega$  reaction we consider two different possibilities: with and without the inclusion of nucleon resonances. The nucleon resonances are included in a way to be consistent with the  $\pi^-p \rightarrow \omega n$  reaction. It is shown that the inclusion of nucleon resonances can describe the data better overall than without their inclusion. However, the SATURNE data in the range of excess energies  $Q < 31$  MeV are still underestimated by about a factor of two. As for the  $pp \rightarrow pp\phi$  reaction it is found that the presently limited available data from DISTO can be reproduced by four sets of values for the vector and tensor  $\phi NN$  coupling constants. Further measurements of the energy dependence of the total cross section near threshold energies should help to constrain better the  $\phi NN$  coupling constant.

PACS number(s): 25.40.Ve, 24.10.Jv, 24.30.-v, 13.75.Cs

## I. INTRODUCTION

Heavy meson production in nucleon nucleon ( $NN$ ) collisions can, in principle, provide important information about the short-range part of the  $NN$  interaction [1]. For example, the  $NN \rightarrow NN\omega/\phi$  reactions at their threshold energies probe distances between the two colliding nucleons of about 0.2 fm [2]. The distance corresponds to the “overlapping region” of the two interacting nucleons, in contrast to the distance of about 0.5 fm probed by much lighter pion production [3]. Therefore, investigation of such heavy meson production reactions should ultimately provide relevant information for testing QCD-based  $NN$  interactions.

Recently, there has been considerable interest in the vector mesons  $\omega$  and  $\phi$ , in connection with the OZI rule [4] violation, and in the strangeness content of the nucleon wave function [5–7]. For example, the Crystal Barrel experiments at LEAR (CERN) [8] found a strong violation of the OZI rule in the  $\phi/\omega$  production rate in antiproton-proton ( $\bar{p}p$ ) annihilation. Furthermore, it was also found that the  $\phi$  to  $\omega$  production ratio in the  $pp \rightarrow pp\omega/\phi$

reactions was enhanced by about an order of magnitude relative to the OZI prediction after correcting for the available phase space volume [9]. These findings may be interpreted as a considerable admixture of the  $s\bar{s}$  configuration in the nucleon wave function.

Another item of interest in  $\omega$  meson production processes is the so-called “missing resonances” problem, where constituent quark models predict more states than have been observed experimentally [10,11]. This has been attributed to the possibility that many such missing resonances couple either weakly or not at all to the  $\pi N$  channel, but may couple more strongly or exclusively to the  $\omega N$  channel. Indeed, some theoretical studies of  $\omega$  photoproduction were made [12,13] inspired by this possibility.

Although, so far, no baryon resonances have been observed to decay into the  $\omega N$  channel, some theoretical efforts have been made to estimate the coupling strengths of  $\omega$  to the experimentally observed resonances [14–16]. One of the motivations for such a study is the possibility to account for the observed enhancement of the low-mass dilepton pair production in heavy ion collisions [17]. Alternatively, the downward shift of the  $\rho$  and  $\omega$  meson masses (but a smaller shift for the  $\phi$  meson mass) in the nuclear medium [18–22] is also considered as a possible source of the observed enhancement. Indeed if the downward shift is large enough,  $\omega$  meson is expected to form meson-nucleus bound states [23–25]. In any case a better understanding of the vector meson production mechanism in free space is a prerequisite to study such in-medium effects, and also to study the possible couplings of the  $\omega$  meson to (missing) resonances. However, in spite of the pronounced interest in the vector mesons  $\rho$ ,  $\omega$  and  $\phi$ , so far there exist only a limited number of theoretical studies of the near-threshold  $pp \rightarrow pp\omega$  [26–30] and  $pp \rightarrow pp\phi$  [26,31,32] reactions. This situation also holds for the near-threshold  $pn \rightarrow d\omega/\phi$  [33,34] and  $pd \rightarrow {}^3\text{He}\omega$  [35] reactions.

From the experimental side, apart from the old data at high excess energies [36], only the total cross section data from SATURNE [37] were available until recently for  $pp \rightarrow pp\omega$  in the near-threshold region with excess energies below  $Q = 31$  MeV. There are also total cross section and angular distribution data at excess energy  $Q = 319$  MeV from the DISTO Collaboration [9]. Recently the COSY-TOF Collaboration has measured the total cross section for  $pp \rightarrow pp\omega$  at two excess energies,  $Q = 92$  and 173 MeV [38]. These fill in partly the energy gap between the SATURNE and DISTO data, and are critical in studying the energy dependence of the total cross section in the extended near-threshold region. In addition to the total cross sections, the COSY-TOF Collaboration has also measured the angular distribution of the  $\omega$  meson produced at  $Q = 173$  MeV. As has been pointed out in Ref. [27], the angular distribution plays a major role in disentangling different reaction mechanisms. These new data from the COSY-TOF Collaboration, together with earlier data [37], offer the opportunity to investigate the  $pp \rightarrow pp\omega$  reaction more in detail than has been done previously. Thus, in the present study we focus on the near-threshold  $pp \rightarrow pp\omega$  reaction in free space. We study this reaction by considering two different possibilities: with and without the inclusion of nucleon resonances [30]. The possibility of a large, off-shell  $S_{11}(1535)$  resonance contribution has been considered recently by the Tübingen group [29].

In the present work we also consider the  $pp \rightarrow pp\phi$  reaction. The only data available for this reaction near-threshold energies are the reanalyzed total cross section and angular distribution from the DISTO Collaboration at  $Q = 83$  MeV [9]. These data are not sufficient to provide stringent constraints on theoretical models. In studying the  $pp \rightarrow pp\phi$  reaction we do not consider the possibility of nucleon resonances, because not enough data exist to

either draw any meaningful conclusions about their role, or to fix new parameters associated with the resonances. (Also note that no baryon resonances have been observed decaying into the  $\phi N$  channel.)

To study the  $pp \rightarrow pp\omega/\phi$  reactions, we use a relativistic effective Lagrangian at the hadronic level, where the reaction amplitude is calculated within the distorted wave Born approximation, including both the initial and final state  $pp$  interactions (denoted by ISI and FSI, respectively). The ISI is implemented in the on-shell approximation [2,30,39,40], while the FSI is generated using the Bonn  $NN$  potential model [41]. The finite width of the  $\omega$ , which is very important near threshold energies, is also included. The  $\omega p$  FSI is included only via the pole diagrams (s-channel processes). Many of the cut-off parameters and coupling constants necessary for the present study have already been fixed from other reactions in previous studies [2,27,31,39]. It turns out that the  $pp \rightarrow pp\omega$  reaction is apparently described better with the inclusion of nucleon resonances. However, in order to draw a definite conclusion we need more data for exclusive observables in the energy region above, but close to  $Q = 30$  MeV. This is because there is no established method to remove the multi-pion background associated with the  $\omega$ -meson width from the raw data in order to extract the cross sections. The finite  $\omega$  width is very important for energies  $Q < 30$  MeV and can possibly make the extracted data strongly dependent on the model used in the analysis [37]. As for the  $pp \rightarrow pp\phi$  reaction, we definitely need more data to constrain the model parameters.

This article is organized as follows. In Section II the general structure of the reaction amplitude in the present approach is explained. In Section III we discuss the  $pp \rightarrow pp\omega$  reaction without the inclusion of nucleon resonances; in Section IV we discuss the reaction with the inclusion of nucleon resonances. Section V treats the  $pp \rightarrow pp\phi$  reaction. The results are discussed and summarized in Section VI.

## II. STRUCTURE OF REACTION AMPLITUDE

In this section we describe the structure of the reaction amplitude for the  $NN \rightarrow NNV$  ( $V = \omega, \phi$ ) reaction following Ref. [39], to make this article self-contained.

In Fig. 1 we show a decomposition of the reaction amplitude for the  $NN \rightarrow NNV$  ( $V = \omega, \phi$ ) reactions. The reaction amplitude is calculated in the distorted wave Born approximation using a relativistic meson exchange model. We begin by considering the meson-nucleon ( $MN$ ) and  $NN$  interactions as the building blocks. Then, we consider all possible combinations of these building blocks in a topologically distinct way, with two nucleons in the initial state, and two nucleons plus a meson in the final state. Here diagrams leading to double counting, e.g., those contributing to mass and vertex renormalizations must be excluded, since we use the physical masses and coupling constants. The ellipsis in Fig. 1 indicates those diagrams that are more involved, or higher orders, which are not included in this work. In particular, we neglect the  $MN$  FSI, which otherwise would be generated by solving the three-body Faddeev equation.

In order to make use of the available potential models of  $NN$  scattering, we perform the calculation within a three-dimensional formulation which is obtained from the Bethe-Salpeter equation by maintaining the relativistic unitarity and Lorentz covariance of the resulting amplitude. We follow the procedure of Blankenbecler and Sugar [42] as adopted

in the Bonn  $NN$  potential model [41]. The vector meson production amplitude,  $M$ , may be written as

$$M = (1 + T_f^{(-)\dagger} iG_f^{(-)*})(\epsilon^* \cdot J)(1 + iG_i^{(+)} T_i^{(+)}) , \quad (1)$$

where  $T_{(i,f)}$  stands for the  $NN$   $T$ -matrix in the initial( $i$ )/final( $f$ ) state,  $G_{(i,f)}$  is the three-dimensional Blankenbecler-Sugar (BBS) propagator, and  $\epsilon^*$  is the polarization vector of the vector meson produced. The superscript  $\pm$  in  $T_{(i,f)}$  and  $G_{(i,f)}$  indicates the boundary conditions,  $(-)$  for incoming and  $(+)$  for outgoing waves. The production current  $J^\mu$ , which is the  $MN$   $T$ -matrix with one of the meson legs attached to a nucleon (first diagram on the r.h.s. in Fig. 1) is defined by

$$J^\mu = \sum_{M'} [T_{(MN \leftarrow M'N)}]_1 iP_{M'} [\Gamma_{M'NN}^\mu]_2 + (1 \leftrightarrow 2) , \quad (2)$$

where  $T_{(MN \leftarrow M'N)}$  stands for the  $MN$   $T$ -matrix describing the transition  $M'N \rightarrow MN$ , and  $\Gamma_{M'NN}^\mu$  and  $P_{M'}$  are respectively the  $M'NN$  vertex and the corresponding meson propagator. The subscripts 1 and 2 denote the two interacting nucleons 1 and 2. The summation is over the intermediate mesons  $M'$ . We note that if the four dimensional full two-nucleon propagator is used, the reaction amplitude given by Eq. (1) would have an additional term to avoid the double counting arising from the term involving  $iG_i^{(+)} T_i^{+}$  and/or  $iG_f^{(+)} T_f^{+}$  and the current  $J^\mu$ , since  $J^\mu$  also contains meson-exchange  $NN$  interactions. This additional term vanishes when we use the reduced three dimensional propagator  $G_{(i/f)}$  which restricts the energy of the propagating two nucleons to be on their respective mass shells.

In the near-threshold energy region, the two nucleon energy in the final state  $f$  is very low and hence the  $NN$  FSI amplitude,  $T_f^{(-)\dagger}$  in Eq. (1), can be calculated from a number of realistic  $NN$  potential models. In the present work we use the Bonn  $NN$  potential model [41]. This model is defined by a reduced three dimensional BBS version of the Bethe-Salpeter equation,

$$T = \mathcal{V} + \mathcal{V} iG T , \quad (3)$$

where  $G$  denotes the BBS two-nucleon propagator, consistent with those appearing in Eq. (1). (Note that the factor  $-i$  difference in the definitions of  $\mathcal{V}$  and  $T$  from those in Ref. [41].)

For the  $NN \rightarrow NN\omega/\phi$  reactions the  $NN$  initial state interaction (ISI) amplitude,  $T_i^{(+)}$  in Eq. (1), must be calculated at incident beam energies above 1.89 and 2.59 GeV, respectively. There exists no accurate  $NN$  interaction model with which one can perform calculations reliably at such high incident beam energies. In the present work we follow Ref. [40], and make the on-shell approximation to evaluate the ISI contribution, which was also applied in the study of the  $NN \rightarrow NN\eta$  reaction [39]. This amounts to keeping only the  $\delta$ -function part of the Green function  $G_i$  in evaluating the loop integral involving  $iG_i^{(+)} T_i^{(+)}$  in Eq. (1). The required on-shell  $NN$  ISI amplitude is calculated from Ref. [43]. As discussed in Ref. [40], this is a reasonable approximation to the full  $NN$  ISI. In this approximation the basic effect of the  $NN$  ISI is to reduce the magnitude of the meson production cross section [39,44]. In fact, it is easy to see that the angle-integrated production cross section in each partial wave state  $j$  is reduced by a factor  $\lambda_j$  [40]:

$$\lambda_j = \left| \frac{1}{2} (\eta_j(p) e^{i2\delta_j(p)} + 1) \right|^2$$

$$= \eta_j(p) \cos^2(\delta_j(p)) + \frac{1}{4} [1 - \eta_j(p)]^2 \leq \frac{1}{4} [1 + \eta_j(p)]^2 , \quad (4)$$

where  $\delta_j(p)$  and  $\eta_j(p)$  denote respectively the phase shift and corresponding inelasticity, and  $p$  is the relative momentum of the two nucleons in the initial state. The  $NN$  ISI has been considered fully by Batinić et al. [44] in the study of the  $pp \rightarrow pp\eta$  reaction, whose threshold corresponds to an incident energy of about 1.25 GeV. Their results support the on-shell approximation used in the present work. Quite recently, Baru et al. [45] have also investigated the effects of the  $NN$  ISI in the  $NN \rightarrow NN\eta$  reaction. Although there are obviously (off-shell) effects which are absent in the on-shell approximation, the results of Ref. [45] also show that the bulk of the  $NN$  ISI effect is accounted for in the on-shell approximation. In particular, we do not expect the off-shell effects of the ISI to change the conclusion of the present work.

Next, we consider the production current  $J^\mu$  defined by Eq. (2) based on meson exchange models. Following Refs. [31,39,46], we split the  $MN$   $T$ -matrix in Fig. 1 into the pole ( $T_{MN}^P$ ) and non-pole ( $T_{MN}^{NP}$ ) parts and calculate the non-pole part in the Born approximation. Then, the  $MN$   $T$ -matrix can be written as [47]

$$T_{MN} = T_{MN}^P + T_{MN}^{NP} , \quad (5)$$

where

$$T_{MN}^P = \sum_B f_{MNB}^\dagger i g_B f_{MNB} , \quad (6)$$

with  $f_{MNB}$  and  $g_B$  denoting the dressed meson-nucleon-baryon ( $MNB$ ) vertex and baryon propagator, respectively. The summation is over the relevant baryons  $B$ . The non-pole part of the  $T$ -matrix is given by

$$T_{MN}^{NP} = V_{MN}^{NP} + V_{MN}^{NP} i G T_{MN}^{NP} , \quad (7)$$

where  $V_{MN}^{NP} \equiv V_{MN} - V_{MN}^P$ , with  $V_{MN}^P$  denoting the pole part of the full  $MN$  potential  $V_{MN}$ .  $V_{MN}^P$  is given by an equation analogous to Eq. (6) with the dressed vertices and propagators replaced by the corresponding bare vertices and propagators. We neglect the second term of Eq. (7) and hence the full  $MN$   $T$ -matrix in Eq. (2) is approximated as  $T_{MN} \cong T_{MN}^P + V_{MN}^{NP}$ .

With the approximation described above, the resulting current  $J^\mu$  consists of baryonic and mesonic ( $J_{mec}^\mu$ ) currents. The baryonic current is further divided into the nucleonic ( $J_{nuc}^\mu$ ) and nucleon resonance ( $J_{res}^\mu$ ) currents, so that the total current is written by

$$J^\mu = J_{nuc}^\mu + J_{res}^\mu + J_{mec}^\mu . \quad (8)$$

The vector meson production currents are illustrated diagrammatically in Fig. 2, where  $V$  stands for the  $\omega$  or  $\phi$  meson. Note that they are all Feynman diagrams and, as such, they include both the positive- and negative-energy propagation of the intermediate state particles. The nucleonic current is constructed consistently with the  $NN$  potential in Eq. (3). For the mesonic current, it turns out that we may consider only the  $V\rho\pi$  ( $V = \omega, \phi$ )

exchange-current contribution for both the  $pp \rightarrow pp\omega/\phi$  reactions. The nucleon resonance current  $J_{res}^\mu$ , included only in the  $pp \rightarrow pp\omega$  reaction, is explained in Section IV.

Here, some general remarks on the meson production currents are in order [39]. As a consequence of using a three-dimensional reduction of Bethe-Salpeter equation, the definition of the energy (time component) for the intermediate state particles in the production currents becomes ambiguous. In order to be consistent with the  $NN$  interaction used in the present work, we follow the BBS three-dimensional reduction prescription: (1) The energy of a virtual meson at the  $MNN$  vertex is taken to be  $q_0 = \varepsilon(p) - \varepsilon(p')$ , where  $\varepsilon(p)[\varepsilon(p')]$  is the energy of the nucleon before [after] the emission of the virtual meson, with  $\varepsilon(p) \equiv \sqrt{p^2 + m_N^2}$ . (2) The energy of the intermediate state baryon in the nucleonic and resonance currents are taken to be  $p_0 = \omega(k) + \varepsilon(p')$  at the  $B \rightarrow M + N$  vertex, while at the  $N \rightarrow M + B$  vertex it is taken to be  $p_0 = \varepsilon(p') - \omega(k)$ , where  $\omega(k)$  is the energy of the meson produced in the final state. The BBS reduction prevents three particle cuts which occur in a more exact calculation.

### III. $PP \rightarrow PP\omega$ WITHOUT RESONANCE

In this Section, we consider the  $pp \rightarrow pp\omega$  reaction without the inclusion of nucleon resonances. Then, the total  $\omega$ -meson production current  $J^\mu$  may be given by the sum of the nucleonic and  $\omega\rho\pi$  meson-exchange currents,  $J^\mu = J_{nuc}^\mu + J_{mec}^\mu$ , as shown in Fig. 2 ( $V = \omega$ ).

The nucleonic current  $J_{nuc}^\mu$  is defined by

$$J_{nuc}^\mu = \sum_{j=1,2} \left( \Gamma_j^\mu iS_j U + U iS_j \Gamma_j^\mu \right) , \quad (9)$$

with  $\Gamma_j^\mu$  denoting the  $\omega NN$  vertex and  $S_j$  the nucleon (Feynman) propagator for the nucleon  $j$ . The summation is over the two interacting nucleons, 1 and 2.  $U$  stands for the meson-exchange  $NN$  potential which is, in principle, identical to the driving potential  $\mathcal{V}$  used in the construction of the  $NN$  interaction (Eq. (3)), except that here meson retardation effects are retained following the Feynman prescription.

The  $\omega$  production vertex  $\omega NN$ ,  $\Gamma_j^\mu$  in Eq. (9), is obtained from the Lagrangian density,

$$\mathcal{L}(x) = -\bar{\psi}_N(x) \left( g_{\omega NN} [\gamma_\mu - \frac{\kappa_\omega}{2m_N} \sigma_{\mu\nu} \partial^\nu] \omega^\mu(x) \right) \psi_N(x) , \quad (10)$$

where  $m_N$ ,  $\psi_N(x)$  and  $\omega^\mu(x)$  stand for the nucleon mass, nucleon and  $\omega$ -meson fields, respectively.  $g_{\omega NN}$  denotes the vector coupling constant and  $\kappa_\omega \equiv f_{\omega NN}/g_{\omega NN}$  ( $g_{\omega NN} \neq 0$ ), with  $f_{\omega NN}$  the tensor coupling constant.  $J_{nuc}^\mu$  defined by Eq. (9) is illustrated in Fig. 2a.

As in most meson-exchange models of hadronic interactions, each hadronic vertex is accompanied by a form factor in order to account for the composite or finite-size nature of the hadrons involved. Thus, the  $\omega NN$  vertex obtained from the above Lagrangian is multiplied by a form factor [31,39],

$$F_{\omega NN}(p^2) = \frac{\Lambda_N^4}{\Lambda_N^4 + (p^2 - m_N^2)^2} , \quad (11)$$

where  $p^2$  is the four-momentum squared of either the incoming or outgoing off-shell nucleon. It is normalized to unity when the nucleon is on its mass shell,  $p^2 = m_N^2$ . Following Ref. [31], we adopt  $g_{\omega NN} = 9.0$  in Eq. (10). The vector to tensor coupling constant ratio,  $\kappa_\omega$ , is not well established; in fact the values quoted in literature are relatively small and vary in a range,  $-0.16 \pm 0.01 \leq \kappa_\omega \leq +0.14 \pm 0.20$  [27]. Therefore, we consider  $\kappa_\omega$  and  $\Lambda_N$ , respectively in Eqs. (10) and (11), as free parameters in the present work.

The  $\omega\rho\pi$  vertex for  $\omega$  production in the meson-exchange current,  $J_{mec}^\mu$  (Fig. 2b), is derived from the Lagrangian density,

$$\mathcal{L}_{\omega\rho\pi}(x) = \frac{g_{\omega\rho\pi}}{\sqrt{m_\omega m_\rho}} \varepsilon_{\alpha\beta\nu\mu} \partial^\alpha \vec{\rho}^\beta(x) \cdot \partial^\nu \vec{\pi}(x) \omega^\mu(x), \quad (12)$$

where  $\varepsilon_{\alpha\beta\nu\mu}$  is the totally antisymmetric Levi-Civita tensor with  $\varepsilon_{0123} = -1$ . The  $\omega\rho\pi$  vertex obtained from the above Lagrangian is multiplied by a form factor,

$$F_{\omega\rho\pi}(q_\rho^2, q_\pi^2) \equiv F_\rho(q_\rho^2) F_\pi(q_\pi^2) = \left( \frac{\Lambda_\rho^2}{\Lambda_\rho^2 - q_\rho^2} \right) \left( \frac{\Lambda_\pi^2 - m_\pi^2}{\Lambda_\pi^2 - q_\pi^2} \right), \quad (13)$$

where  $\Lambda_\omega \equiv \Lambda_\rho = \Lambda_\pi$  is assumed [31]. It is normalized to unity at  $q_\rho^2 = 0$  and  $q_\pi^2 = m_\pi^2$ , consistent with the kinematics at which the coupling constant  $g_{\omega\rho\pi}$  is extracted.

The meson-exchange current is given by

$$J_{mec}^\mu = [\Gamma_{\rho NN}^\alpha(q_\rho)]_1 i D_{\alpha\beta}(q_\rho) \Gamma_{\omega\rho\pi}^{\beta\mu}(q_\rho, q_\pi, k_\omega) i \Delta(q_\pi) [\Gamma_{\pi NN}(q_\pi)]_2 + (1 \leftrightarrow 2), \quad (14)$$

where  $D_{\alpha\beta}(q_\rho)$  and  $\Delta(q_\pi)$  stand for the  $\rho$ - and  $\pi$ -meson (Feynman) propagators, respectively. The vertices  $\Gamma$  involved are self-explanatory. The coupling constant,  $g_{\omega\rho\pi} = 10.0$  in Eq. (12), has been fixed from a systematic study of pseudoscalar and vector meson radiative decays combined with the vector meson dominance assumption [31,48]. Its sign is fixed from a study of pion photoproduction in the 1 GeV energy region [49]. The  $\rho NN$  and  $\pi NN$  vertices in Eq. (14) are consistent with those in the Bonn-B  $NN$  potential [41], except that here we use the pseudovector coupling instead of the pseudoscalar coupling for the  $\pi NN$  vertex. In addition, the cut-off parameter,  $\Lambda_{\pi NN} = 1300$  MeV, is adopted at the  $\pi NN$  vertex. We are, then, left with the cut-off parameter  $\Lambda_\rho = \Lambda_\pi$  in Eq. (13) which will be treated as a free parameter in the present work.

Next, we explain how the model parameters  $\kappa_\omega$ ,  $\Lambda_N$ , and  $\Lambda_\rho = \Lambda_\pi$  are determined in the present approach. In Ref. [27] it was pointed out that the angular distribution of the emitted  $\omega$  mesons is a sensitive quantity for determining the *absolute amount* of nucleonic as well as mesonic current contributions in addition to the relative sign of the two amplitudes. This was also demonstrated in Refs. [30,50]. (The value quoted in Ref. [50] should read  $g_{\omega NN} = +9.0$ .) Furthermore, the shape of the  $\omega$  angular distribution is particularly sensitive to the value of  $\kappa_\omega$ , the tensor to vector coupling ratio [30,50]. Thus, we can make use of both the  $\omega$  angular distribution and total cross section data from COSY-TOF [38] at  $Q = 173$  MeV to fix these three parameters. We obtain a reasonable fit to the data with the values,  $\Lambda_\rho = \Lambda_\pi = 1000$  MeV,  $\Lambda_N = 1190$  MeV and  $\kappa_\omega \simeq -2.0$ . Table I summarizes all the parameter values within the approach in this Section. Here, it should be mentioned that, at  $Q = 173$  MeV, the energy involved in the final  $pp$  subsystem extends beyond the pion threshold. The  $NN$  FSI used in the present work has been developed to fit the phase-shifts only up to the pion production

threshold. Therefore, strictly, we are beyond the applicability of this interaction. However, the final  $pp$  energy involved is not large enough to introduce any significant deviation.

The  $\kappa_\omega$  dependence of the  $\omega$  angular distribution is illustrated in Fig. 3. Here, since the mesonic current contribution gives a flat angular distribution, and because we are interested in the  $\kappa_\omega$  dependence of the shape, we have kept the mesonic current contribution unchanged ( $\Lambda_\rho = \Lambda_\pi = 1000$  MeV) and varied both  $\kappa_\omega$  and  $\Lambda_N$ . The latter parameter has to be varied in order to keep the total cross section fixed. The results show indeed the shape is sensitive to the value of  $\kappa_\omega$ . Note in particular that values of  $\kappa_\omega > -1$  are clearly unable to reproduce the data. We note here that the value of the tensor coupling,  $f_{\omega NN} = 0$ , in the Bonn  $NN$  potential used in the FSI in the present work, is quite different from the value of  $f_{\omega NN} = \kappa_\omega g_{\omega NN} \simeq -2.0 \times 9 = -18$  used to reproduce the angular distribution data. However, the exchanged  $\omega$  meson in the Bonn  $NN$  potential model is associated with the virtual  $\omega$  meson and represents the isoscalar-vector quantum numbers exchanged, and is not necessarily related to the physical  $\omega$  meson.

Next, in order to see how the shape of the  $\omega$  angular distribution is sensitive to the value of  $g_{\omega NN}$ , we keep the value,  $\kappa_\omega = -2.0$  fixed, which reproduces the  $\omega$  angular distribution very well, and calculate the  $\omega$  angular distribution for different values of  $g_{\omega NN}$ . Here again the mesonic current contribution has been kept fixed. We show in Fig. 4 (the right panel) the result obtained using the value,  $(g_{\omega NN})^2/4\pi = (17.37)^2/4\pi = 24$ , approximately the value used in the Bonn  $NN$  potential, together with one of the reasonable fits (the left panel) obtained with  $g_{\omega NN} = 9.0$ . Recall that the total cross section is normalized in both calculations. The result obtained with  $(g_{\omega NN})^2/4\pi = 24$  also gives a good fit to the data, where the change in the coupling constant  $g_{\omega NN}$ ,  $9.0 \rightarrow 17.37$ , is compensated by the change in the cut-off parameter  $\Lambda_N$ ,  $1190 \rightarrow 1020$  MeV. This implies that, for a given mesonic current contribution, the shape of the  $\omega$  angular distribution is not sensitive to the value of  $g_{\omega NN}$ , but is sensitive to the value of  $\kappa_\omega$ . This implies that the different momentum dependence introduced via the tensor coupling to the nucleonic current plays an important role to the shape of the  $\omega$  angular distribution.

With all the parameters fixed, we next study the energy dependence of the total cross section. In Fig. 5 we show the predicted energy dependence of the total cross section with various effects: (1) effects of the finite  $\omega$  width denoted by “width”, (2) the initial and final state  $pp$  interactions denoted by “ISI” and “FSI”, respectively, and (3) using a constant matrix element denoted by “Phase space”, where “ $(\epsilon^* \cdot J) = \text{constant}$ ” is used in Eq. (1). The results with “ISI+FSI+width” in Fig. 5 (the bottom-right panel) include all the effects considered in the present model, and should be compared with the data. Recall that the present parameters are adjusted so as to reproduce the total cross section of  $30.8\mu b$  and the  $\omega$  angular distribution at  $Q = 173$  MeV. In Fig. 5, we also show the result of Ref. [37] denoted by “Hibou et al.” used in the analysis of the SATURNE data. Obviously, the present result underestimates the SATURNE data [37] to a large extent in the range of excess energies,  $Q < 31$  MeV. The reason for this discrepancy can be attributed to an overestimate of the mesonic current contribution as fixed at  $Q = 173$  MeV. This results in a substantial reduction of the cross section close to threshold, due to a much stronger destructive interference between the nucleonic and mesonic current contributions as the excess energy decreases. In fact, the large overestimation of the mesonic current can be verified from the  $\pi^- p \rightarrow \omega n$  reaction. With all the parameters fixed to reproduce the



$pp \rightarrow pp\omega$  at  $Q = 173$  MeV, we have looked at the model prediction of the energy dependence of the  $\pi^-p \rightarrow \omega n$  total cross section. It turns out that the model largely overestimates the data from Ref. [60] as the center-of-mass energy  $W$  increases due to the rapidly increasing  $\omega\rho\pi$  exchange current contribution. We were unable to reproduce both the  $pp \rightarrow pp\omega$  data at  $Q = 173$  MeV and the energy dependence of the  $\pi^-p \rightarrow \omega n$  total cross section within our approach which considers only the nucleonic and mesonic currents.

In an attempt to improve the agreement in the present approach, we have investigated the effect of different form factors for the vector and tensor couplings at the  $\omega$  production vertex in the nucleonic current. Different momentum dependences of the vector ( $F_1$ ) and the tensor ( $F_2$ ) strong form factors at the  $\omega NN$  meson production vertex are quite possible. In particular, recent experimental results from the Jefferson Lab [52] for the ratio of the proton electric and magnetic form factors,  $\mu_p G_{Ep}(Q^2)/G_{Mp}(Q^2)$  ( $\mu_p$ : proton magnetic moment), show a linear decrease as the four-momentum transfer squared ( $Q^2$ ) increases, namely, the vector ( $F_1$ ) to the tensor ( $F_2$ ) electromagnetic ratio is,  $F_2(Q^2)/F_1(Q^2) \sim 1/Q$  [53], which shows that  $F_1$  and  $F_2$  have different momentum dependences. (The perturbative QCD predicts  $F_2(Q^2)/F_1(Q^2) \sim 1/Q^2$  [54].) Using different cut-off values for the vector and tensor form factors, respectively,  $\Lambda_{Nv} = 1300$  MeV and  $\Lambda_{Nt} = 1600$  MeV, and using the same functional form of Eq. (11), we have recalculated the energy dependence of the total cross section. Note that these parameters together with other parameters,  $\Lambda_\rho = \Lambda_\pi = 1450$  MeV and  $\kappa_\omega = -0.5$ , can reproduce the  $\omega$  angular distribution data at  $Q = 173$  MeV reasonably well. However, the predicted cross section is enhanced by only  $10 \sim 20$  % at near threshold energies, and still underestimates substantially all the SATURNE data points [37]. We have also considered a possible contribution of the  $\omega\sigma\sigma$  mesonic current contribution by assigning reasonable range of values for the coupling constants and cut-off parameters associated with this current. But this also gives only a small contribution. Thus, within the approach of considering only the contributions from the nucleonic and mesonic currents, it seems unlikely to be able to reproduce the measured energy dependence of the total cross section in the range of excess energies  $Q \leq 173$  MeV. Of course, we could fix the model parameters by fitting the total cross section at a lower excess energy point. However, the model would then overestimate the total cross sections near  $Q = 173$  MeV substantially, and also it would be difficult to reproduce the  $\omega$  angular distribution at  $Q = 173$  MeV.

Apart from the difficulties mentioned above, we also note that the rather large (negative) value of  $\kappa_\omega = -2.0$  required to reproduce the  $\omega$  angular distribution, is not easily reconciled with other nuclear processes. For example, such a large value of  $\kappa_\omega$  leads to a rather strong  $NN$  (isoscalar) tensor force. This will affect the  $NN$  tensor force, given primarily by the  $\pi$  and  $\rho$  meson exchange, in such a way that it becomes extremely difficult to describe  $NN$  scattering and deuteron properties. In fact, a rough calculation [51] shows that it is nearly impossible to describe the  $NN$  phase-shift data with such a strong tensor coupling ( $f_{\omega NN} = \kappa_\omega g_{\omega NN} \simeq -18$ ).

Thus, although there is currently no definite experimental evidence for the  $\omega$  meson to couple to any nucleon resonance, it would be natural to expect that some resonance currents give contributions, since high nucleon incident energies are involved in the near-threshold  $\omega$  production in  $pp$  collisions. The reduction of the mesonic current at high excess energies may then be compensated by the nucleon resonance current contributions. We study such a possibility in Section IV.

#### IV. $PP \rightarrow PP\omega$ WITH RESONANCE

In order to limit the number of resonances considered and thereby avoid the introduction of an excessive number of new parameters, we restricted the resonances to those: (1) that appreciably decay to the  $N + \gamma$  channel so that the vector meson dominance (VMD) assumption may be used to produce  $\omega$ , (2) whose mass distributions confined around  $(m_N + m_\omega)$  and therefore contribute maximally at near threshold energies, (3) that can describe consistently the  $\pi^- p \rightarrow \omega n$  reaction. In addition, to see if a dominant  $S_{11}(1535)$  resonance contribution as reported in Ref. [29] is possible, and since many parameters associated with  $S_{11}(1535)$  are under better control than those for other higher resonances, we also include this resonance in the present study. As a result, we consider contributions from the following four nucleon resonances,  $S(1535)(\frac{1}{2}^-)****$ ,  $P(1710)(\frac{1}{2}^+)***$ ,  $D(1700)(\frac{3}{2}^-)***$  and  $P(1720)(\frac{3}{2}^+)****$ , where we list the spin, parity and status of the corresponding resonances explicitly [55]. The construction of the resonance current, and the associated details are given in Ref. [39].

The resonance current  $J_{res}^\mu$  contribution to the  $pp \rightarrow pp\omega$  reaction arises from the spin-1/2 ( $J_{1/2res}^\mu$ ) and spin-3/2 ( $J_{3/2res}^\mu$ ) resonance currents in the present approach:

$$J_{res}^\mu = J_{1/2res}^\mu + J_{3/2res}^\mu . \quad (15)$$

The spin-1/2 resonance current, in analogy to the nucleonic current, is defined by

$$J_{1/2res}^\mu = \sum_{j=1,2} \sum_{N^*} \left( \Gamma_{\omega j N^*}^\mu i S_{N^*} U_{N^*} + \tilde{U}_{N^*} i S_{N^*} \Gamma_{\omega j N^*}^\mu \right) . \quad (16)$$

Here  $\Gamma_{\omega j N^*}^\mu$  stands for the  $\omega NN^*$  vertex involving the nucleon  $j$ .  $S_{N^*}(p) = (\not{p} + m_{N^*})/(p^2 - m_{N^*}^2 + im_{N^*}\Gamma_{N^*})$  is the  $N^*$  resonance propagator, with  $m_{N^*}$  and  $\Gamma_{N^*}$  denoting the mass and width of the resonance, respectively. The summation is over the two interacting nucleons,  $j = 1$  and  $2$ , and also over the spin-1/2 resonances,  $N^* = S_{11}(1535)$  and  $P_{11}(1710)$ . In Eq. (16)  $U_{N^*}$  ( $\tilde{U}_{N^*}$ ) stands for the  $NN \rightarrow NN^*$  ( $NN^* \rightarrow NN$ ) meson-exchange transition potential, and is given by

$$U_{N^*} = \sum_{\substack{M=\pi,\eta \text{ for } S_{11}(1535) \\ M=\pi,\eta,\sigma \text{ for } P_{11}(1710)}} \Gamma_{MNN^*}(q) i \Delta_M(q^2) \Gamma_{MNN}(q) + \sum_{M=\rho,\omega} \Gamma_{MNN^*}^\mu(q) i D_{\mu\nu(M)}(q) \Gamma_{MNN}^\nu(q), \quad (17)$$

where  $\Delta_M(q^2)$  and  $D_{\mu\nu(M)}(q)$  are the (Feynman) propagators of the exchanged pseudoscalar (scalar) and vector mesons, respectively.  $\Gamma_{MNN}(q)$  and  $\Gamma_{MNN}^\mu(q)$  denote the pseudoscalar (scalar) and vector  $MNN$  vertex, respectively. These vertices are taken consistently with the  $NN$  potential  $\mathcal{V}$  appearing in Eq. (3), except for the type of coupling at the  $\pi NN$  vertex and the  $\omega NN$  coupling constant. Following Ref. [39], we use the pseudovector-coupling instead of the pseudoscalar-coupling at the  $\pi NN$  vertex, which is consistent with the chiral constraints in the lowest order [56]. We also follow the discussion in Refs. [27,31,46], and use the value of the  $\omega NN$  coupling constant,  $g_{\omega NN} = 11.76$ . These exceptions also apply to the spin-3/2 resonance current,  $J_{3/2res}^\mu$ . An analogous expression to Eq. (17) also holds for  $\tilde{U}_{N^*}$ . In Eq. (17) we have an extra,  $\sigma$ -meson exchange in the  $NP_{11}(1710) \leftrightarrow NN$  transition potential, since the  $P_{11}(1710) \rightarrow N\pi\pi$  decay branch is relatively large [55]. Thus, we simulate these two pions conveniently by a  $\sigma$ -meson.

Following Refs. [14,39,57,58], the transition vertices  $\Gamma_{MNN^*}$  and  $\Gamma_{MNN^*}^\mu$  in Eqs. (16) and (17) for spin-1/2 resonances are obtained from the interaction Lagrangian densities,

$$\mathcal{L}_{\eta NN^*}^{(\pm)}(x) = \mp g_{\eta NN^*} \bar{\psi}_{N^*}(x) \left\{ \left[ i\lambda \Gamma^{(\pm)} + \left( \frac{1-\lambda}{m_{N^*} \pm m_N} \right) \Gamma_\mu^{(\pm)} \partial^\mu \right] \eta(x) \right\} \psi_N(x) + h.c. , \quad (18a)$$

$$\mathcal{L}_{\pi NN^*}^{(\pm)}(x) = \mp g_{\pi NN^*} \bar{\psi}_{N^*}(x) \left\{ \left[ i\lambda \Gamma^{(\pm)} + \left( \frac{1-\lambda}{m_{N^*} \pm m_N} \right) \Gamma_\mu^{(\pm)} \partial^\mu \right] \vec{\tau} \cdot \vec{\pi}(x) \right\} \psi_N(x) + h.c. , \quad (18b)$$

$$\mathcal{L}_{\sigma NP_{11}}(x) = g_{\sigma NP_{11}} \bar{\psi}_{P_{11}}(x) \sigma \psi_N(x) + h.c. , \quad (18c)$$

$$\mathcal{L}_{\omega NN^*}^{(\pm)}(x) = \left( \frac{g_{\omega NN^*}}{m_{N^*} + m_N} \right) \bar{\psi}_{N^*}(x) \left\{ \left[ \frac{\Gamma_\mu^{(\mp)} \partial^2}{m_{N^*} + m_N} + \Gamma^{(\mp)} (-i\partial_\mu + \kappa_\omega \sigma_{\mu\nu} \partial^\nu) \right] \omega^\mu(x) \right\} \psi_N(x) + h.c. , \quad (18d)$$

$$\mathcal{L}_{\rho NN^*}^{(\pm)}(x) = \left( \frac{g_{\rho NN^*}}{m_{N^*} + m_N} \right) \bar{\psi}_{N^*}(x) \left\{ \left[ \frac{\Gamma_\mu^{(\mp)} \partial^2}{m_{N^*} + m_N} + \Gamma^{(\mp)} (-i\partial_\mu + \kappa_\rho \sigma_{\mu\nu} \partial^\nu) \right] \vec{\tau} \cdot \vec{\rho}^\mu(x) \right\} \psi_N(x) + h.c. , \quad (18e)$$

where  $\vec{\pi}(x)$ ,  $\omega^\mu(x)$ ,  $\vec{\rho}^\mu(x)$  and  $\psi_{N^*}(x)$  denote the  $\pi$ ,  $\omega$ ,  $\rho$  and spin-1/2 nucleon resonance fields, respectively. The upper and lower signs refer to the even(+) and odd(-) parity resonances, respectively. The operators  $\Gamma^{(\pm)}$  and  $\Gamma_\mu^{(\pm)}$  in Eqs. (18a) - (18e) are defined by

$$(\Gamma^{(+)}, \Gamma^{(-)}, \Gamma_\mu^{(+)}, \Gamma_\mu^{(-)}) = (\gamma_5, 1, \gamma_5 \gamma_\mu, \gamma_\mu) . \quad (19)$$

The parameter  $\lambda$  in Eqs. (18a) and (18b) controls the admixture of the two types of couplings: pseudoscalar (ps-coupling:  $\lambda = 1$ ) and pseudovector (pv-coupling:  $\lambda = 0$ ) for an even parity resonance and, scalar ( $\lambda = 1$ ) and vector ( $\lambda = 0$ ) for an odd parity resonance, where both choices of the parameter  $\lambda$  give equivalent results when baryons are on their mass shells. In this work we take  $\lambda = 0$ . Note that in principle we should not allow only the pure  $\Gamma_\mu^{(\mp)}$  coupling in Eqs. (18d) and (18e), because unlike the  $VNN$  vertex ( $V$ =vector meson), this coupling alone at the  $VNN^*$  vertex prevents us from estimating its strength using the VMD, since it violates gauge invariance. In the present work, we use a more general gauge invariant Lagrangian density as used in Ref. [58] based on Ref. [14].

Similar to the case of spin-1/2 resonances, the spin-3/2 resonance current is defined by

$$J_{3/2res}^\mu = \sum_{j=1,2} \sum_{N^*} \left( \Gamma_{\omega j N^*}^{\mu\alpha} i S_{\alpha\beta(N^*)} U_{N^*}^\beta + \tilde{U}_{N^*}^\alpha i S_{\alpha\beta(N^*)} \Gamma_{\omega j N^*}^{\beta\mu} \right) . \quad (20)$$

Here  $\Gamma_{\omega j N^*}^{\beta\mu}$  stands for the  $\omega NN^*$  vertex function involving the nucleon  $j$ .  $S_{\alpha\beta(N^*)}(p) = (\not{p} + m_{N^*}) \{ -g_{\alpha\beta} + \gamma_\alpha \gamma_\beta / 3 + (\gamma_\alpha p_\beta - p_\alpha \gamma_\beta) / 3m_{N^*} + 2p_\alpha p_\beta / 3m_{N^*}^2 \} / (p^2 - m_{N^*}^2 + im_{N^*} \Gamma_{N^*})$  is the spin-3/2 Rarita-Schwinger propagator. The summation is over the two interacting nucleons,  $j = 1$  and  $2$ , and also over the spin-3/2 resonances,  $N^* = D_{13}(1700)$  and  $P_{13}(1720)$ . In Eq. (20)  $U_{N^*}^\alpha$  ( $\tilde{U}_{N^*}^\alpha$ ) stands for the  $NN \rightarrow NN^*$  ( $NN^* \rightarrow NN$ ) meson-exchange transition potential, and is given by

$$U_{N^*}^\alpha = \sum_{M=\pi,\eta} \Gamma_{MNN^*}^{\alpha\lambda}(q) i \Delta_M(q^2) \Gamma_{MNN}(q) + \sum_{M=\rho,\omega} \Gamma_{MNN^*}^{\alpha\lambda}(q) i D_{\lambda\nu(M)}(q) \Gamma_{MNN}^\nu(q) , \quad (21)$$

where  $\Gamma_{MNN^*}^\alpha(q)$  and  $\Gamma_{MNN^*}^{\alpha\lambda}(q)$  denote the pseudoscalar and vector  $MNN^*$  vertices, respectively. An analogous expression to Eq. (21) also holds for  $\tilde{U}_{N^*}^\alpha$ .

The  $MNN^*$  vertices involving spin-3/2 nucleon resonances in Eqs. (20) and (21) are obtained from the Lagrangian densities [39,57],

$$\mathcal{L}_{\eta NN^*}^{(\pm)}(x) = \left( \frac{g_{\eta NN^*}}{m_\eta} \right) \bar{\psi}_{N^*}^\mu(x) \Theta_{\mu\nu}(z) \Gamma^{(\mp)} \psi_N(x) \partial^\nu \eta(x) + h.c. , \quad (22a)$$

$$\mathcal{L}_{\pi NN^*}^{(\pm)}(x) = \left( \frac{g_{\pi NN^*}}{m_\pi} \right) \bar{\psi}_{N^*}^\mu(x) \Theta_{\mu\nu}(z) \Gamma^{(\mp)} \vec{\tau} \psi_N(x) \cdot \partial^\nu \vec{\pi}(x) + h.c. , \quad (22b)$$

$$\begin{aligned} \mathcal{L}_{\omega NN^*}^{(\pm)}(x) = & \mp i \left( \frac{g_{\omega NN^*}^{(1)}}{2m_N} \right) \bar{\psi}_{N^*}^\mu(x) \Theta_{\mu\nu}(z) \Gamma_\lambda^{(\pm)} \psi_N(x) \omega^{\lambda\nu}(x) \\ & - \left( \frac{g_{\omega NN^*}^{(2)}}{4m_N^2} \right) (\partial_\lambda \bar{\psi}_{N^*}^\mu(x) \Theta_{\mu\nu}(z) \Gamma^{(\pm)} \psi_N(x)) \omega^{\lambda\nu}(x) + h.c. , \end{aligned} \quad (22c)$$

$$\begin{aligned} \mathcal{L}_{\rho NN^*}^{(\pm)}(x) = & \mp i \left( \frac{g_{\rho NN^*}^{(1)}}{2m_N} \right) \bar{\psi}_{N^*}^\mu(x) \Theta_{\mu\nu}(z) \Gamma_\lambda^{(\pm)} \vec{\tau} \psi_N(x) \cdot \vec{\rho}^{\lambda\nu}(x) \\ & - \left( \frac{g_{\rho NN^*}^{(2)}}{4m_N^2} \right) (\partial_\lambda \bar{\psi}_{N^*}^\mu(x) \Theta_{\mu\nu}(z) \Gamma^{(\pm)} \vec{\tau} \psi_N(x)) \cdot \vec{\rho}^{\lambda\nu}(x) + h.c. , \end{aligned} \quad (22d)$$

where  $\Theta_{\mu\nu}(z) \equiv g_{\mu\nu} - (z + 1/2)\gamma_\mu\gamma_\nu$ , and  $\omega^{\lambda\nu}(x) \equiv \partial^\lambda \omega^\nu(x) - \partial^\nu \omega^\lambda(x)$  and  $\vec{\rho}^{\lambda\nu}(x) \equiv \partial^\lambda \vec{\rho}^\nu(x) - \partial^\nu \vec{\rho}^\lambda(x)$ . In order to reduce the number of parameters, we take  $z = -1/2$  in the present work.

Following Ref. [39], the relevant coupling constants associated with the resonance currents are calculated utilizing the Particle data [55] whenever available; they are determined from the centroid values of the extracted partial decay widths (and masses) of the resonances. Those couplings involving vector mesons, are estimated from the corresponding radiative decay width in conjunction with the VMD. In order to reduce the number of free parameters, the ratio of the  $VNN^*$  ( $V = \rho, \omega$ ) coupling constants for the spin-3/2 resonances,  $D_{13}(1700)$  and  $P_{13}(1720)$ , have been fixed to be  $g_{VNN^*}^{(1)}/g_{VNN^*}^{(2)} = -2.1$ , the same ratio as that for  $g_{\gamma NP_{33}}^{(1)}/g_{\gamma NP_{33}}^{(2)} = -2.1$ , extracted from the ratio of  $E2/M1 \cong -2.5\%$  determined from pion photoproduction measurements [59].

Following Refs. [39,46], and in complete analogy to the nucleonic current, we introduce the off-shell form factors at each vertex involved in resonance currents. We adopt the same form factor as given by Eq. (11), with  $m_N$  replaced by  $m_{N^*}$  at the  $MNN^*$  vertex, in order to account for the  $N^*$  resonance being off-shell. The  $MNN^*$  vertex, where the exchanged meson is also off-shell, is multiplied by an extra form factor  $F_M(q^2)$  in order to account for the meson being off-shell (see Eqs. (17) and (21)). The corresponding full form factor is, therefore, given by the product  $F_N(p^2)F_M(q^2)$ , where  $M$  stands for the exchanged meson between the two interacting nucleons. The form factor  $F_M(q^2)$  is taken consistently with the  $NN$  potential  $\mathcal{V}$  in Eq. (3); the only two differences are the normalization point of  $F_{\rho,\omega}(q^2)$  and the cutoff parameter value of  $F_\pi(q^2)$ . Here, the form factor for vector mesons  $F_{\rho,\omega}(q^2)$  is normalized to unity at  $q^2 = 0$  in accordance with the kinematics at which the coupling constant  $g_{\rho,\omega NN^*}$  was extracted, i.e.,  $F_{\rho,\omega}(q^2) = (\Lambda_{\rho,\omega}^2/(\Lambda_{\rho,\omega}^2 - q^2))^2$ . For the pion form factor

$F_\pi(q^2)$  we use the cutoff value  $\Lambda_\pi = 900$  MeV. To be consistent in this section, this value (rather than  $\Lambda_\pi = 1300$  MeV) is also used in the form factor at the  $\pi NN$  vertex appearing in the mesonic current constructed.

Since we now include the resonance current, the free parameters in the nucleonic and mesonic currents in the previous Section have to be readjusted. In addition, we will consider the  $\sigma NN^*$  coupling for  $N^* = P_{11}(1710)$  as a free parameter in the present work. In order to fix these free parameters in this Section, we use the  $\pi^- p \rightarrow \omega n$  total cross section data from Ref. [60] (see Ref. [15] for a discussion about the data), in addition to the  $pp \rightarrow pp\omega$  total cross section and angular distribution data from the COSY-TOF Collaboration [38]. We note that at the excess energy of  $Q = 173$  MeV for the  $pp \rightarrow pp\omega$  reaction, the center-of-mass energy  $W$  of the subsystem  $\pi^- p \rightarrow \omega n$  appearing as a building block in the description of the  $pp \rightarrow pp\omega$  reaction, will reach a maximum value of  $W \simeq 1.9$  GeV. Thus, we fix the parameters so as to reproduce the measured energy dependence of the  $\pi^- p \rightarrow \omega n$  total cross section data up to  $W \simeq 1.9$  GeV.

We show in Fig. 6 the calculated energy dependence of the total cross section obtained with a selected parameter set. At lower energies  $W$ ,  $D_{13}(1700)$  and  $P_{13}(1720)$  contributions are dominant, but neither  $S_{11}(1535)$  nor  $P_{11}(1710)$  give appreciable contributions for the  $\pi^- p \rightarrow \omega n$  total cross section. Furthermore, many trial calculations show that, without including the resonances it is very difficult to reproduce the near-threshold behavior of the  $\pi^- p \rightarrow \omega n$  total cross section up to energies  $W \simeq 1.9$  GeV using a reasonable set of parameters. However, with the inclusion of the resonances, we need a somewhat softer (stronger) form factor for the  $\omega\rho\pi$  vertex to fit the overall energy dependence exhibited by the data. In particular, the part of the form factor which accounts for the off-shell behavior of the exchanged  $\rho$  meson requires a dipole form,

$$F_{\omega\rho\pi}(q_\rho^2, q_\pi^2) \equiv F_\rho(q_\rho^2)F_\pi(q_\pi^2) = \left( \frac{\Lambda_\rho^2}{\Lambda_\rho^2 - q_\rho^2} \right)^{n_\rho} \left( \frac{\Lambda_\pi^2 - m_\pi^2}{\Lambda_\pi^2 - q_\pi^2} \right), \quad (23)$$

with  $n_\rho = 2$ ,  $\Lambda_\rho = 850$  MeV and  $\Lambda_\pi = 1450$  MeV. A cutoff parameter value of  $\Lambda_N = 1100$  MeV has been also determined at the  $\omega NN$  meson production vertex. A different form factor,  $\exp(\beta q_\rho^2) \exp(-\alpha W^2)$ , was introduced at the  $\omega\rho\pi$  vertex in Ref. [61] to overcome the difficulties in reproducing the data using the monopole form factor  $F_\rho(q_\rho^2)$  in Eq. (23).

Next, using the  $\omega$  angular distribution data from COSY-TOF [38], we further fix parameters associated with the  $P_{11}(1710)$  resonance, namely, the coupling constant  $g_{\sigma NP_{11}}$  associated with the  $\sigma$  exchange introduced effectively to simulate the observed decay channel,  $P_{11}(1710) \rightarrow N + 2\pi$ . The value for the coupling constant  $g_{\sigma NP_{11}}$  is adjusted to reproduce the  $pp \rightarrow pp\omega$  total cross section of  $30.8\mu b$  at  $Q = 173$  MeV. Thus, in this procedure, the value obtained for  $g_{\sigma NP_{11}}$  is not strictly related to the branching ratio for the  $N + 2\pi$  channel; instead, the contribution from  $P_{11}(1710)$  should be regarded as also taking into account the other possible resonance contributions not included explicitly in our model.

We show in Fig. 7 the  $\omega$  angular distribution calculated by fitting the coupling constant  $g_{\sigma NP_{11}}$  to the total cross section of  $30.8\mu b$ , together with a more reasonable value of  $\kappa_\omega = -0.5$ . Recall that with the value of  $\kappa_\omega \simeq -2.0$  obtained in Section III, it would be very difficult to describe the  $NN$  scattering data consistently [51]. Two values for  $g_{\sigma NP_{11}}$  are found to be able to reproduce the total cross section of  $30.8\mu b$  at  $Q = 173$  MeV. The results for the  $\omega$  angular distribution are shown in Fig. 7, for those obtained with  $g_{\sigma NP_{11}} = -4.3$

(the upper panel) and  $g_{\sigma NP_{11}} = +4.8$  (the lower panel). Although the value,  $g_{\sigma NP_{11}} = +4.8$  reproduces the  $\omega$  angular distribution data from COSY-TOF [38] better, the result for the energy dependence of the total cross section is worse than that with  $g_{\sigma NP_{11}}$ . Thus, we will show only the results obtained with  $g_{\sigma NP_{11}} = -4.3$ . We summarize in Table II all the parameters fixed in the present approach, i.e., with the inclusion of the nucleon resonances.

Next, in Fig. 8 we show the energy dependence of the  $pp \rightarrow pp\omega$  total cross section calculated using the fixed parameters in Table II. The result is greatly improved compared to that without the inclusion of any nucleon resonances studied in Section III. (See Fig. 5.) However, it still underestimates the SATURNE data [37], which are in the range of excess energies  $Q < 31$  MeV, by about a factor of two. Thus, further investigation is needed to understand better the near-threshold  $pp \rightarrow pp\omega$  reaction. As already mentioned, we also need more data for exclusive observables in the energy region above but close to  $Q = 30$  MeV, because there is no established method for removing the multi-pion background associated with the  $\omega$ -meson width from the raw data to extract the cross sections. The effect of the width is very important in the energy region,  $Q < 30$  MeV, and the extraction of the cross section can become highly model dependent.

Considering the results shown in Fig. 8, one possibility for improving the agreement with the data would be to introduce extra resonances, which enhance the total cross section at near threshold energies but only moderately enhance at excess energies around  $Q = 173$  MeV, if such adequate candidates exist. However, on the other hand, the introduction of new resonances would introduce more ambiguities. The other effect to be investigated is the  $\omega N$  FSI, which is expected to enhance the total cross sections at near threshold energies, because a QCD sum rule study of the meson-nucleon spin-isospin averaged scattering lengths for the vector mesons  $\rho, \omega$  and  $\phi$ , suggests attractive  $VN$  ( $V = \rho, \omega, \phi$ ) interactions [21].

Next, in Fig. 9 we show a decomposition of each resonance contribution to the energy dependence of the  $pp \rightarrow pp\omega$  total cross section. Close to threshold energies the dominant contribution comes from  $D_{13}(1700)$ , while at higher excess energies, the dominant contribution comes from  $P_{11}(1710)$ , although the contribution of this resonance was negligible in the  $\pi^- p \rightarrow \omega n$  reaction. Here, again the  $S_{11}(1535)$  resonance contribution is very small in our model. We should mention that we also studied the contribution from the  $S_{11}(1650)$  resonance in the present approach, but it did not give an appreciable contribution. Thus, if we want to be consistent with both the  $\pi^- p \rightarrow \omega n$  and  $pp \rightarrow pp\omega$  reactions, it appears necessary to include at least three nucleon resonances,  $P_{11}(1710)$ ,  $D_{13}(1700)$  and  $P_{13}(1720)$ , in the present approach.

## V. $PP \rightarrow PP\phi$ WITHOUT RESONANCE

The  $pp \rightarrow pp\phi$  reaction can be treated in an analogous way to the  $pp \rightarrow pp\omega$  reaction in Section III, namely, considering only the nucleonic ( $J_{nuc}^\mu$ ) and mesonic ( $J_{mec}^\mu$ ) current contributions. However, the scarcity of data, especially in the near-threshold region, makes this study more difficult. In fact there is only one total cross section and one angular distribution available near-threshold at an excess energy of  $Q = 83$  MeV measured by the DISTO Collaboration [9]. A theoretical study of the  $pp \rightarrow pp\phi$  reaction in Ref. [31] was made within a similar approach to that of the present study, in the sense that it used a relativistic meson-exchange model, considering contributions from the nucleonic and  $\phi\rho\pi$

exchange currents as the dominant contributions. The present study differs from that of Ref [31] in that: (1) the  $\phi$  angular distribution data from DISTO [9] used in this study were reanalyzed [9] and absolute normalization of the corresponding total cross section was established, and (2) the  $pp$  ISI is included explicitly.

The relative importance among the possible meson exchange current contributions was estimated based on an SU(3) effective Lagrangian, together with various effects described in Ref. [31]. Furthermore, the test calculations performed in Ref. [31] showed that the  $\phi\rho\pi$ -exchange current was by far the dominant mesonic current. The *combined* contribution of all other meson-exchange currents to the total cross section is about two orders of magnitude smaller than this. Moreover, possible contributions from meson-exchange currents involving heavy mesons, in particular, the  $\phi\phi f_1$ - and  $\phi\omega f_1$ -exchange currents were also examined using the larger values of the coupling constants calculated from the observed decay of  $f_1 \rightarrow \phi + \gamma$ . However, this contribution, as well as the  $\phi\phi\sigma$ - and  $\phi\omega\sigma$ -exchange currents, also turned out to be negligible [31]. Finally, as in the case of  $\omega$  production, there are neither experimental indications of any of the known isospin-1/2  $N^*$  resonances decaying into the  $N\phi$  channel, nor do there exist enough data for the near-threshold  $pp \rightarrow pp\phi$  reaction to fix the relevant parameters and judge their validities. Thus, we study the  $pp \rightarrow pp\phi$  reaction considering the contributions only from the nucleonic and  $\phi\rho\pi$  mesonic currents.

The coupling constant,  $g_{\phi\rho\pi}$ , associated with the mesonic current  $J_{mec}^\mu$ , can be extracted from the measured branching ratio. Specifically, the coupling constant  $g_{\phi\rho\pi} = -1.64$  is determined directly from the measured decay width of  $\phi \rightarrow \rho + \pi$  [55], where the sign is inferred from SU(3) symmetry [31]. We note that the coupling constant  $g_{\phi\rho\pi} = -1.64$  is extracted at different kinematics compared to that of the  $\omega$ :  $g_{\phi\rho\pi}$  is determined at  $q_\rho^2 = m_\rho^2$  and  $q_\pi^2 = m_\pi^2$ , whereas  $g_{\omega\rho\pi}$  is extracted at  $q_\rho^2 = 0$  and  $q_\pi^2 = m_\pi^2$ . Then, the corresponding form factor (cf. Eq. (13)) is defined by

$$F_{\phi\rho\pi}(q_\rho^2, q_\pi^2) \equiv F_\rho(q_\rho^2)F_\pi(q_\pi^2) = \left( \frac{\Lambda_\rho^2 - m_\rho^2}{\Lambda_\rho^2 - q_\rho^2} \right) \left( \frac{\Lambda_\pi^2 - m_\pi^2}{\Lambda_\pi^2 - q_\pi^2} \right). \quad (24)$$

In Eq. (24) we again assume the cut-off parameter  $\Lambda_\phi \equiv \Lambda_\rho = \Lambda_\pi$  corresponds to those in Eq. (13).

Although we do not have to use the same parameters for the  $\phi$  production as those used in the  $pp \rightarrow pp\omega$  reaction, we use the same value  $\Lambda_N = 1190$  MeV for the cut-off parameter in the  $\phi NN$  meson production vertex, because the  $\phi\rho\pi$  exchange current gives the dominant contribution to the total cross section, and reproducing the absolute normalization of the total cross section is relatively insensitive to the cut-off parameter  $\Lambda_N$  in the nucleonic current compared to the cut-off parameters in the  $\phi\rho\pi$  vertex form factors. Therefore, we have three free parameters to be adjusted to reproduce the  $\phi$  meson production total cross section and angular distribution data [9], namely,  $g_{\phi NN}$  and  $\kappa_\phi$  in the nucleonic current, after replacing  $\omega \rightarrow \phi$  in Eq. (10), and  $\Lambda_\phi \equiv \Lambda_\rho = \Lambda_\pi$  in the form factor of Eq. (24) in the  $\phi\rho\pi$  mesonic current, after replacing  $\omega \rightarrow \phi$  in Eqs. (12) and (14).

In Figs. 10 and 11 we show the  $\kappa_\phi$  dependence of the calculated  $\phi$  angular distributions, for  $g_{\phi NN} = -0.4$  and  $g_{\phi NN} = -1.6$ , respectively. Results in Fig. 10 imply that as long as the value of  $g_{\phi NN}$  is small, the angular distribution data can be reproduced well within experimental error bars, irrespective of the values of  $\kappa_\phi$  up to  $\kappa_\phi \simeq -4.0$ . On the other hand, results in Fig. 11 show that the larger value,  $g_{\phi NN} = -1.6$  makes the shape of the

calculated  $\phi$  angular distribution sensitive to  $\kappa_\phi$ . One can notice that for a certain value of  $\kappa_\phi$ , the shape of the calculated  $\phi$  angular distribution changes from convex to concave. After some test calculations, we find the optimum value for this transition is roughly  $\kappa_\phi \simeq -2.0$ . Thus, around  $\kappa_\phi \simeq -2.0$  we can expect that there are a large number of possibilities for the values of  $g_{\phi NN}$  and  $\Lambda_\phi$  which can reproduce the experimentally observed flat  $\phi$  angular distribution [9].

Next, we fix the value  $\kappa_\phi = -2.0$  (and  $\Lambda_N = 1190$  MeV), and study the  $g_{\phi NN}$  dependence of the  $\phi$  angular distribution. Some of the calculated results are shown in Fig. 12. Note that, the top-right panel in Fig. 12 has a contribution solely from the mesonic current ( $g_{\phi NN} = 0$ ), which, neglecting the  $\phi - \omega$  mixing and the OZI-allowed two step processes [31], may be regarded as the limiting case of no  $s\bar{s}$  component in the nucleon wave function, if the value of  $g_{\phi NN}$  is considered as a measure for the  $s\bar{s}$  component. Since we have not included quark degrees of freedom explicitly, it is difficult to draw a definite conclusion on the  $s\bar{s}$  component in the nucleon wave function. We summarize in Table III the four possible parameter sets for  $g_{\phi NN}$ ,  $\kappa_\phi$  and  $\Lambda_\phi$  fixed by fitting the DISTO  $\phi$  angular distribution data [9]. They all reproduce the experimental data [9] reasonably well. This suggests that one needs to study additional observables, e.g., the energy dependence of the  $pp \rightarrow pp\phi$  total cross section, in order to constrain better the parameters of the model.

Here, it may be interesting to compare the values of  $g_{\phi NN}$  and  $\kappa_\phi$  obtained in the present work with those extracted in Ref. [64] by studying the off-shell time-like nucleon form factors using the  $p(\gamma, e^+e^-)p$  reaction. They obtained  $(g_{\phi NN}, \kappa_\phi) \simeq (1.3, 7.2)$ . (Note that their definition of  $\kappa_\phi$  is different from that of the present study by a factor  $4m_N/m_\phi$  ( $m_{N,\phi}$ : masses of the nucleon and  $\phi$  meson); for comparison, this factor is included in the value of  $\kappa_\phi$  here.)

Next, using the four parameter sets given in Table III, we study the energy dependence of the  $pp \rightarrow pp\phi$  total cross section. We show the calculated results in Fig. 13. The results exhibit very similar energy dependences for the parameter sets  $(g_{\phi NN}, \kappa_\phi) = (0.0, 0.0), (-0.4, -0.5)$  and  $(-0.4, -4.0)$ , while that for  $(-2.0, -2.0)$  shows a different dependence especially at excess energies in the region  $Q < 50$  MeV. Thus, measuring the energy dependence of the total cross section for  $Q < 50$  MeV will help constrain better the model parameters, in particular, the magnitude of the coupling constant  $g_{\phi NN}$ .

## VI. SUMMARY AND DISCUSSION

We have studied the  $pp \rightarrow pp\omega/\phi$  reactions using a relativistic effective Lagrangian at the hadronic level, including both the initial and final state  $pp$  interactions. For both reactions we have made use of the recently measured  $\omega$  and  $\phi$  angular distributions in addition to the total cross section data to fix the model parameters.

We have studied the  $pp \rightarrow pp\omega$  reaction considering two possibilities, i.e., the  $\omega$  meson is produced by: (1) the nucleonic and mesonic current contributions, and (2) the nucleonic, mesonic and nucleon resonance current contributions. The results show that the energy dependence of the total cross section in the range of excess energies  $Q \leq 173$  MeV, is apparently described better by the inclusion of nucleon resonances, which is implemented in a way to be consistent with the  $\pi^-p \rightarrow \omega n$  reaction. However, the calculation still underestimates the SATURNE data by about a factor of two, where the data points are in



the range of excess energies  $Q < 31$  MeV. This remains still a problem in understanding the reaction mechanism. In this connection, we need more data for exclusive observables in the energy region above, but close to  $Q = 30$  MeV because there is no established method for removing the multi-pion background associated with the  $\omega$ -meson width from the raw data. This removal is necessary for extracting the cross sections in the energy region,  $Q < 30$  MeV, where the effect of the width is very important, and the extraction can be highly model dependent.

In connection with studying resonance contributions to the  $pp \rightarrow pp\omega$  reaction, we plan to investigate the  $p\omega$  invariant mass distributions for this reaction [62]. A measurement of the invariant mass distributions for this reaction, should give significant information as to whether contributions from resonances are appreciable or not. Such theoretical studies have been made for the  $pp \rightarrow pp\eta$  [58], and  $pp \rightarrow p\Lambda K^+$  [63] reactions. Thus, the study of the invariant mass distributions may be an alternative method for studying the possible  $\omega$ -meson (and  $\phi$ -meson) resonance couplings both theoretically and experimentally.

In addition to the  $pp \rightarrow pp\omega$  reaction, we have studied the  $pp \rightarrow pp\phi$  reaction considering the contributions solely from the nucleonic and mesonic current contributions. Because of the scarcity of data for this reaction in the near threshold energy region, we have obtained four parameter sets which can reproduce the  $\phi$  angular distribution data from DISTO [9] equally well. Predictions for the energy dependence of the  $pp \rightarrow pp\phi$  total cross section indicate that a measurement of the cross section close to threshold should be able to constrain better the coupling constant  $g_{\phi NN}$  ( $\simeq 0$  or  $\simeq -2$ ).

Finally, although there exists an enormous interest in vector meson properties in highly complicated many-nucleon environments, e.g., dilepton production in heavy ion collisions and meson ( $\omega$ ) nuclear bound states, the data for the  $NN \rightarrow NNV$  reaction ( $V$ : vector meson) are currently inadequate for understanding the production mechanism of these mesons in free space. Thus, more measurements of vector meson production in free space, and especially in  $NN$  collisions, may be a first step towards understanding the properties of vector mesons in such complicated nuclear environments.

### Acknowledgment:

We would like to thank C. Wilkin and F. Hibou for useful discussions, and providing us the code used in the analysis of the SATURNE data [37]. Our thanks also go to K.-Th. Brinkmann for providing us the  $\omega$  angular distribution data of the COSY-TOF Collaboration [38], and to J. Haidenbauer for helpful discussions. We also thank W.G. Love for a careful reading of the manuscript. This work is supported by Forschungszentrum-Jülich, contract No. 41445282 (COSY-058).

## REFERENCES

- [1] For a recent review on close-to-threshold meson production in hadronic interactions, see, e.g., P. Moskal, M. Wolke, A. Khoukaz, W. Oelert, hep-ph/0208002, to be published in Part. Nucl. Phys. **49** (2002);  
H. Machner and J. Haidenbauer, J. Phys. **G 25**, R231 (1999).
- [2] K. Nakayama, nucl-th/0108032, in the Proceedings of the Symposium on “Threshold Meson Production in  $pp$  and  $pd$  Interaction”, Schriften des Forschungszentrums Jülich, Matter and Materials, **11**, 119 (2002).
- [3] T.-S.H. Lee and D.O. Riska, Phys. Rev. Lett. **70**, 2237 (1993);  
C.J. Horowitz, H.O. Meyer, and D.K. Griegel, Phys. Rev. C **49**, 1337 (1994);  
C. Hanhart, J. Haidenbauer, and J. Speth, Nucl. Phys. **A631**, 515c (1998); C. Hanhart et al., Phys. Lett. B **358**, 21 (1995);  
Y. Maeda, N. Matsuda, and K. Tamura, Nucl. Phys. **A684**, 392c (2001).
- [4] S. Okubo, Phys. Lett. **B5**, 165 (1963);  
G. Zweig, CERN Report No.8419/TH412 (1964);  
I. Iizuka, Prog. Theor. Phys. Suppl. **37 & 38**, 21 (1966).
- [5] For a review, e.g., V.P. Nomokonov, M.G. Sapozhnikov, hep-ph/0204259.
- [6] H.J. Lipkin, Phys. Lett. **60B**, 371 (1976).
- [7] J. Ellis, M. Karliner, D.E. Kharzeev, M.G. Sapozhnikov, Phys. Lett. B **353**, 319 (1995);  
Nucl. Phys. **A673**, 256 (2000).
- [8] C. Amster, Rev. Mod. Phys. **70**, 1293 (1998).
- [9] (a) DISTO Collaboration, F. Balestra et al., Phys. Rev. C **63**, 024004 (2001); (b) Phys. Rev. Lett. **81**, 4572 (1998).
- [10] N. Isgur, G. Karl, Phys. Rev. D **18**, 4187 (1978); *ibid.* **19**, 2653 (1979); *ibid.* **23**, 817(E) (1981);  
R. Koniuk, N. Isgur, *ibid.* **21**, 1868 (1980).
- [11] S. Capstick, W. Roberts, Phys. Rev. D **49**, 4570 (1994); nucl-th/0008028, submitted to Prog. Part. Nucl. Phys.;  
S. Capstick, Phys. Rev. D **46**, 2864 (1992).
- [12] Q. Zhao, Z. Li, C. Bennhold, Phys. Lett. B **436**, 42 (1998); Phys. Rev. C **58**, 2393 (1998).
- [13] Y. Oh, A.I. Titov, T.-S.H. Lee, Phys. Rev. C **63**, 025201 (2001).
- [14] D.O. Riska, G.E. Brown, Nucl. Phys. **A679**, 577 (2001).
- [15] G. Penner, U. Mosel, Phys. Rev. C **65**, 055202 (2002); nucl-th/0207066.
- [16] A.I. Titov, T.-S.H. Lee, Phys. Rev. C **66**, 015204 (2002).
- [17] G. Agakichiev et al. (CERES Coll.), Phys. Rev. Lett. **75**, 1272 (1995); Phys. Lett. B **422**, 405 (1998);  
B. Lenkeit et al. (CERES Coll.), Nucl. Phys. **A661** 23c (1999);  
M. Masera (HELIOS-3 Coll.), Nucl. Phys. **A590**, 93c (1995);  
W.K. Wilson et al. (The DLS Coll.), Phys. Rev. C **57**, 1865 (1998).
- [18] G.E. Brown, M. Rho, Phys. Rev. Lett. **66**, 2720 (1991).
- [19] T. Hatsuda, S.H. Lee, Phys. Rev. C **46**, R34 (1992); T. Hatsuda, S.H. Lee, and H. Shiomi, Phys. Rev. C **52**, 3364 (1995).
- [20] M. Asakawa, C.M. Ko, P. Lévai, X.J. Qiu, Phys. Rev. C **46**, R1159 (1992);  
M. Asakawa and C.M. Ko, Phys. Rev. C **48**, R526 (1993).

- [21] Y. Koike and A. Hayashigaki, Prog. Theor. Phys. **98**, 631 (1997).
- [22] F. Klingl, T. Waas, W. Weise, Phys. Lett. B **431**, 254 (1998).
- [23] K. Tsushima, D.H. Lu, A.W. Thomas, K. Saito, Phys. Lett. B **443**, 26 (1998);  
K. Saito, K. Tsushima, D.H. Lu, and A.W. Thomas, Phys. Rev. C **59**, 1203 (1999);  
K. Tsushima, Nucl. Phys. **A670**, 198 (2000); in the proceedings ISHEPP 98, Dubna,  
Russia, 17 - 22 August 1998, nucl-th/9811063; Nucl. Phys. **A670**, 198 (2000); K.  
Tsushima et al., Nucl. Phys. **A680**, 279 (2001); K. Tsushima, hep-ph/0206069, Proceed-  
ings of the Joint CSSM/JHF/NITP Workshop on Physics at JHF, Adelaide, Australia,  
2002, p. 303.
- [24] R.S. Hayano, S. Hirenzaki, A. Gillitzer, Eur. Phys. J A **6**, 99 (1999).
- [25] F. Klingl, T. Waas, W. Weise, Nucl. Phys. **A650**, 299 (1999).
- [26] A.A. Sibirtsev, Nucl. Phys. **A604**, 455 (1996).
- [27] K. Nakayama et al., Phys. Rev. C **57**, 1580 (1998).
- [28] N. Kaiser, Phys. Rev. C **60**, 057001 (1999).
- [29] C. Fuchs et al., Phys. Rev. C **67**, 025202 (2003).
- [30] K. Tsushima, and K. Nakayama, nucl-th/0211065, to be published in the proceedings of  
the XVIth International Conference on Particles and Nuclei (PANIC02), Osaka, Japan,  
30 September - 4 October 2002.
- [31] K. Nakayama et al., Phys. Rev. C **60**, 055209 (1999).
- [32] A.I. Titov, B. Kämpfer, and V.V. Shklyar, Phys. Rev. C **59**, 999 (1999);  
A.I. Titov, B. Kämpfer and B.L. Reznik, Eur. Phys. J. **A7**, 543 (2000).
- [33] K. Nakayama, J. Haidenbauer, and J. Speth, Phys. Rev. C **63**, 015201 (2000); Nucl.  
Phys. **A689**, 402c (2001).
- [34] V. Yu. Grishina, L.A. Kondratyuk, and M. Büscher, Phys. Atomic Nuclei, **63**, 1824  
(2000).
- [35] R. Wurzing et al., Phys. Rev. C **51**, R443 (1995).
- [36] V. Flaminio et al., CERN preprint CERN-HERA 8401 (1984);  
R. Baldi et al., Phys. Lett. **68B**, 381 (1977).
- [37] F. Hibou et al., Phys. Rev. Lett. **83**, 492 (1999);  
F. Hibou and C. Willkin, private communications.
- [38] S. Abd El-Samad et al. (COSY-TOF Coll.), Phys. Lett. B **522**, 16 (2001).
- [39] K. Nakayama, J. Speth and T.-S. H. Lee, Phys. Rev. C **65**, 045210 (2002).
- [40] C. Hanhart and K. Nakayama, Phys. Lett. B **454**, 176 (1999).
- [41] J. Haidenbauer, private communication; We use the modified version of the Bonn-B  
 $pp$  potential, which is constrained to the low-energy  $pp$  scattering length by a minor  
readjustment of the coupling constant  $g_{\sigma NN}$ , following Phys. Rev. C **40**, 2465 (1989);  
R. Machleidt, potential B (Table A.1), Adv. Nucl. Phys. **19**, 189 (1989).
- [42] R. Blankenbecler and R. Sugar, Phys. Rev. **142**, 1051 (1966).
- [43] The CNS Data Analysis Center, <http://gwdac.phys.gwu.edu>.
- [44] M. Batinić, A. Švarc, and T.-S.H. Lee, Phys. Acripta **56**, 321 (1997).
- [45] V. Baru et al., Phys. Rev. C **67**, 024002 (2003).
- [46] K. Nakayama et al., Phys. Rev. C **61**, 24001 (1999).
- [47] B. C. Pearce and I. R. Afnan, Phys. Rev. C **34**, 991 (1986).
- [48] J.W. Durso, Phys. Lett. B **184**, 348 (1987).
- [49] H. Garcilazo and E. Moya de Guerra, Nucl. Phys. **A562**, 521 (1993).

- [50] K. Tsushima, hep-ph/0206069, Section 6, Proceedings of the Joint CSSM/JHF/NITP Workshop on Physics at JHF, Adelaide, Australia, 2002, p. 303.
- [51] J. Haidenbauer, private communication.
- [52] M.K. Jones et al. (The Jefferson Lab Hall A Coll.), Phys. Rev. Lett. **84**, 1398 (2000); O. Gayou et al. (The Jefferson Lab Hall A Coll.), Phys. Rev. C **64**, 038202 (2001).
- [53] For recent discussions see, e.g., G.A. Miller, and M.R. Frank, Phys. Rev. C **65**, 065205 (2002).
- [54] S.J. Brodsky and G.R. Farrar, Phys. Rev. D **11**, 1309 (1975).
- [55] Particle Data Group, Phys. Rev. D **66**, (2002); Eur. Phys. J. **C3**, 1 (1998).
- [56] V. Bernard, N. Kaiser, and Ulf-G. Meissner, Int. J. Mod. Phys. **E4**, 193 (1995).
- [57] M. Benmerrouche, N. C. Mukhopadhyay, and J. F. Zhang, Phys. Rev. D **51**, 3237 (1995); J. F. Zhang, N. C. Mukhopadhyay and M. Benmerrouche, Phys. Rev. C **52**, 1134 (1995).
- [58] K. Nakayama, J. Haidenbauer, C. Hanhart, and J. Speth, nucl-th/0302061.
- [59] G. Blanpied et al., Phys. Rev. Lett. **79**, 4337 (1997); R. Beck et al., Phys. Rev. C **61**, 035204 (2000).
- [60] J.S. Danburg et al., Phys. Rev. D **2**, 2564 (1970); D.M. Binnie et al., Phys. Rev. D **8**, 2789 (1973); J. Keyne et al., Phys. Rev. D **14**, 28 (1976); H. Karami et al., Nucl. Phys. **B154**, 503 (1979).
- [61] G.I. Lykasov et al., Eur. Phys. J. A **6**, 71 (1999).
- [62] K. Tsushima, and K. Nakayama, work in progress.
- [63] A. Sibirtsev, K. Tsushima, and A.W. Thomas, Phys. Lett. B **421**, 59 (1998).
- [64] S.R. Cotanch, and R.A. Williams, Phys. Lett. B **549**, 85 (2002).

# TABLES

TABLE I. Model parameters fixed for the  $pp \rightarrow pp\omega$  reaction without the inclusion of nucleon resonances. Below, “Bonn” indicates that the same value in the Bonn  $NN$  potential B (Table A.1) [41] is used.

Vertex	Coupling constant	Cut-off (MeV)
Nucleonic current:	$[f_{\omega NN} = \kappa_{\omega} g_{\omega NN}]$	
$\omega NN$ [ $\omega$ production]	$g_{\omega NN} = 9.0$ $[\kappa_{\omega} = -2.0]$	$\Lambda_N = 1190$ [See Eq. (11).]
$MNN[M = \pi, \eta, \rho, \omega, \sigma, a_0(= \delta)]$	Bonn	Bonn
Mesonic current:		
$\omega\rho\pi$ [ $\omega$ production]	$g_{\omega\rho\pi} = 10.0$	$\Lambda_{\omega} \equiv \Lambda_{\rho} = \Lambda_{\pi} = 1000$ [See Eq. (13).]
$\rho NN$	Bonn	Bonn
$\pi NN$ [pv-coupling]	Bonn	1300

TABLE II. Model parameters fixed for the  $pp \rightarrow pp\omega$  reaction with the inclusion of nucleon resonances. Below, “Bonn” indicates that the same value in the Bonn  $NN$  potential B (Table A.1) [41] is used.

Vertex	Coupling constant	Cut-off (MeV)
Nucleonic current:	$[f_{\omega NN} = \kappa_{\omega} g_{\omega NN}]$	
$\omega NN$ [ $\omega$ production]	$g_{\omega NN} = 9.0$ $[\kappa_{\omega} = -0.5]$	$\Lambda_N = 1100$ [See Eq. (11).]
$MNN[M = \pi, \eta, \rho, \omega, \sigma, a_0(= \delta)]$	Bonn	Bonn
Mesonic current:		
$\omega\rho\pi$ [ $\omega$ production]	$g_{\omega\rho\pi} = 10.0$	$\Lambda_{\rho} = 850, \Lambda_{\pi} = 1450$ [See Eq. (23).]
$\rho NN$	Bonn	Bonn
$\pi NN$ [pv-coupling]	Bonn	900
Spin 1/2 resonance current:	$g_{MNN}, g_{MNN^*}$ $\frac{1}{m_{N^*} + m_N}(g_{\rho, \omega NN^*}, \kappa_{\rho, \omega} g_{\rho, \omega NN^*})$ [See Eqs. (18d) and (18e).]	
$S_{11}(1535), \Gamma = 150$ MeV		
$MNN[M = \pi, \eta, \rho, \omega]$ [ $\pi NN$ (pv-coupling)]	Bonn, but $g_{\omega NN} = 11.76$	Bonn, but $\Lambda_{\pi NN} = 900$
$\pi NS_{11}(1535)$	1.25	900
$\eta NS_{11}(1535)$	2.02	Bonn
$\rho NS_{11}(1535)$	(0.0, -4.50) [fm]	Bonn
$\omega NS_{11}(1535)$	(-0.91, 3.34) [fm]	Bonn
$P_{11}(1710), \Gamma = 100$ MeV		
$MNN[M = \sigma, \pi, \eta, \rho, \omega]$ [ $\pi NN$ (pv-coupling)]	Bonn, but $g_{\omega NN} = 11.76$	Bonn, but $\Lambda_{\pi NN} = 900$
$\sigma NP_{11}(1710)$	-4.30	Bonn
$\pi NP_{11}(1710)$	1.20	900
$\eta NP_{11}(1710)$	4.43	Bonn
$\rho NP_{11}(1710)$	(0.0, 6.70) [fm]	Bonn
$\omega NP_{11}(1710)$	(0.0, -1.04) [fm]	Bonn
Spin 3/2 resonance current:	$g_{MNN}^{(1)}, g_{MNN^*}^{(1)}$ $[g_{\rho, \omega NN^*}^{(1)} / g_{\rho, \omega NN^*}^{(2)} = -2.1]$ [See Eqs. (22c) and (22d).]	
$D_{13}(1700), \Gamma = 100$ MeV		
$MNN[M = \pi, \rho, \omega]$ [ $\pi NN$ (pv-coupling)]	Bonn, but $g_{\omega NN} = 11.76$	Bonn, but $\Lambda_{\pi NN} = 900$
$\pi ND_{13}(1700)$	0.44	900
$\rho ND_{13}(1700)$	1.68	Bonn
$\omega ND_{13}(1700)$	2.64	Bonn
$P_{13}(1720), \Gamma = 150$ MeV		
$MNN[M = \pi, \rho, \omega]$ [ $\pi NN$ (pv-coupling)]	Bonn, but $g_{\omega NN} = 11.76$	Bonn, but $\Lambda_{\pi NN} = 900$
$\pi NP_{13}(1720)$	0.17	900
$\rho NP_{13}(1720)$	-3.73	Bonn
$\omega NP_{13}(1720)$	3.45	Bonn

TABLE III. Model parameters for the  $pp \rightarrow pp\phi$  reaction, for four possible sets by the  $\phi$  angular distribution, denoted by (a), (b), (c) and (d). Below, “Bonn” indicates that the same value in the Bonn  $NN$  potential B (Table A.1) [41] is used.

Vertex	Coupling constant	Cut-off (MeV)
Nucleonic current:	$[f_{\phi NN} = \kappa_{\phi} g_{\phi NN}]$	
$\phi NN$ [ $\phi$ production]	(a) $g_{\phi NN} = 0.0 [\kappa_{\phi} \equiv 0]$	$\Lambda_N = 1190$ [See Eq. (11).]
	(b) $g_{\phi NN} = -0.4 [\kappa_{\phi} = -0.5]$	$\Lambda_N = 1190$
	(c) $g_{\phi NN} = -0.4 [\kappa_{\phi} = -4.0]$	$\Lambda_N = 1190$
	(d) $g_{\phi NN} = -2.0 [\kappa_{\phi} = -2.0]$	$\Lambda_N = 1190$
$MNN[M = \pi, \eta, \rho, \omega, \sigma, a_0(= \delta)]$	Bonn	Bonn
Mesonic current:		$\Lambda_{\phi} \equiv \Lambda_{\rho} = \Lambda_{\pi}$
(a) $\phi\rho\pi$ [ $\phi$ production]	$g_{\phi\rho\pi} = -1.64$	$\Lambda_{\phi} = 1930$ [See Eq. (24).]
(b) $\phi\rho\pi$ [ $\phi$ production]	$g_{\phi\rho\pi} = -1.64$	$\Lambda_{\phi} = 2100$
(c) $\phi\rho\pi$ [ $\phi$ production]	$g_{\phi\rho\pi} = -1.64$	$\Lambda_{\phi} = 1915$
(d) $\phi\rho\pi$ [ $\phi$ production]	$g_{\phi\rho\pi} = -1.64$	$\Lambda_{\phi} = 2200$
$\rho NN$	Bonn	Bonn
$\pi NN$ [pv-coupling]	Bonn	1300

# FIGURES

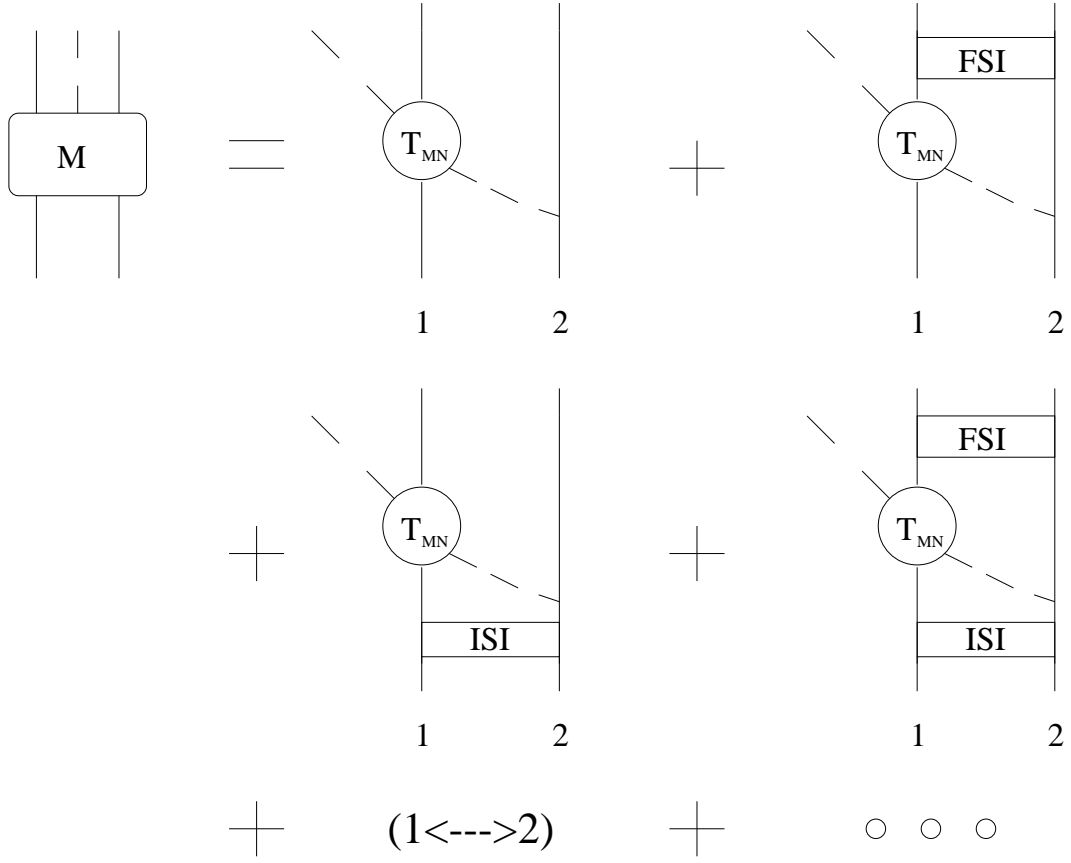


FIG. 1. Decomposition of the reaction amplitude for the  $NN \rightarrow NNV$  ( $V = \omega, \phi$ ) reaction in the present work.  $T_{MN}$  denotes the  $MN$   $T$ -matrix. ISI and FSI stand for the initial and final state  $NN$  interactions, respectively.



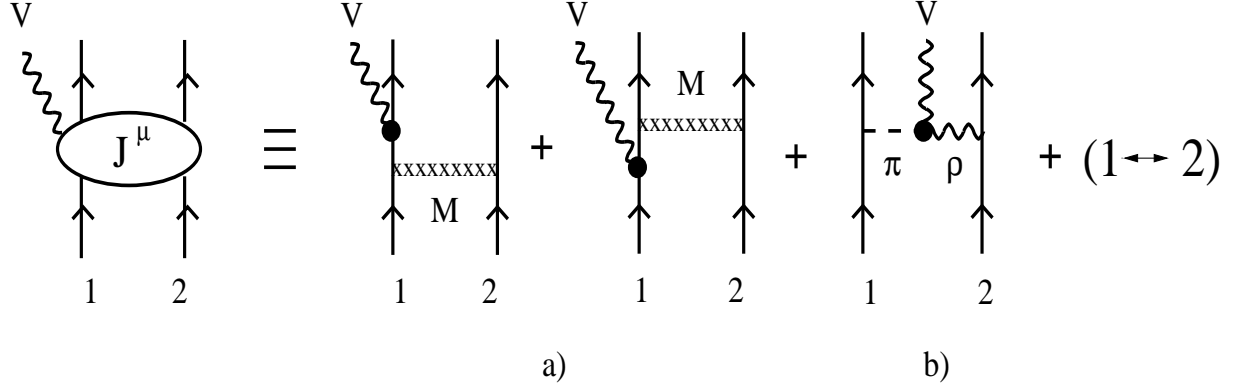


FIG. 2. Vector meson ( $\omega$  or  $\phi$ ) production currents,  $J^\mu$ , included in the present study: a) nucleonic and resonance currents, b) mesonic current.  $V = \omega$  or  $\phi$  and  $M = \pi, \eta, \rho, \omega, \sigma, a_0 (= \delta)$ . In the intermediate states of diagram a), negative-energy propagations for nucleon and resonances are included.

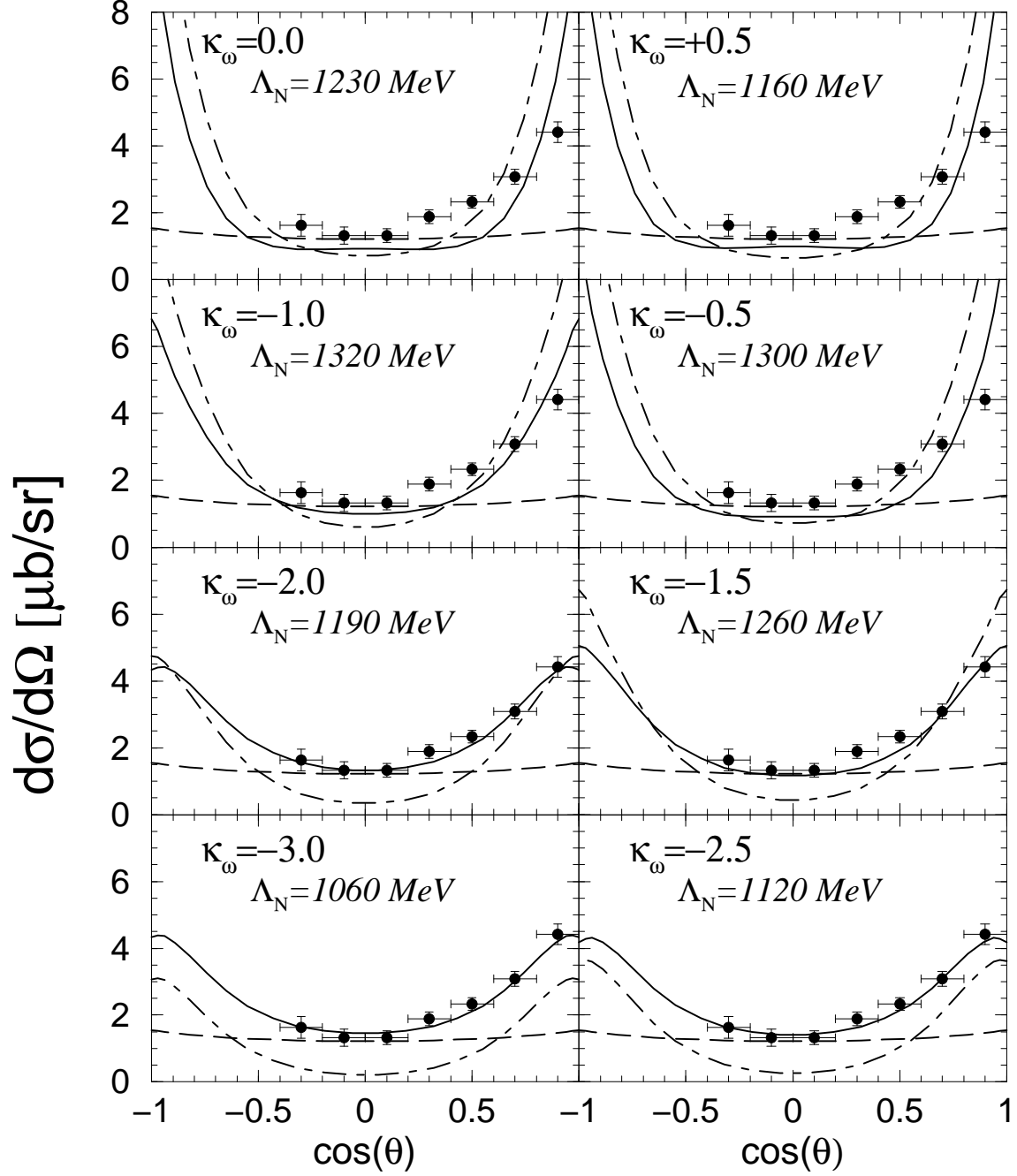


FIG. 3.  $\kappa_\omega$  dependence of the  $\omega$  angular distribution at excess energy  $Q = 173$  MeV, without the inclusion of nucleon resonances. The (dashed, dot-dashed, solid) lines show the (mesonic, nucleonic, total) contributions, respectively. The dots denote data from COSY-TOF [38]. The cut-off parameter  $\Lambda_N$  in the form factor at the  $\omega NN$  production vertex is fitted to the total cross section of  $30.8\mu b$  at excess energy  $Q = 173$  MeV [38] for each panel.

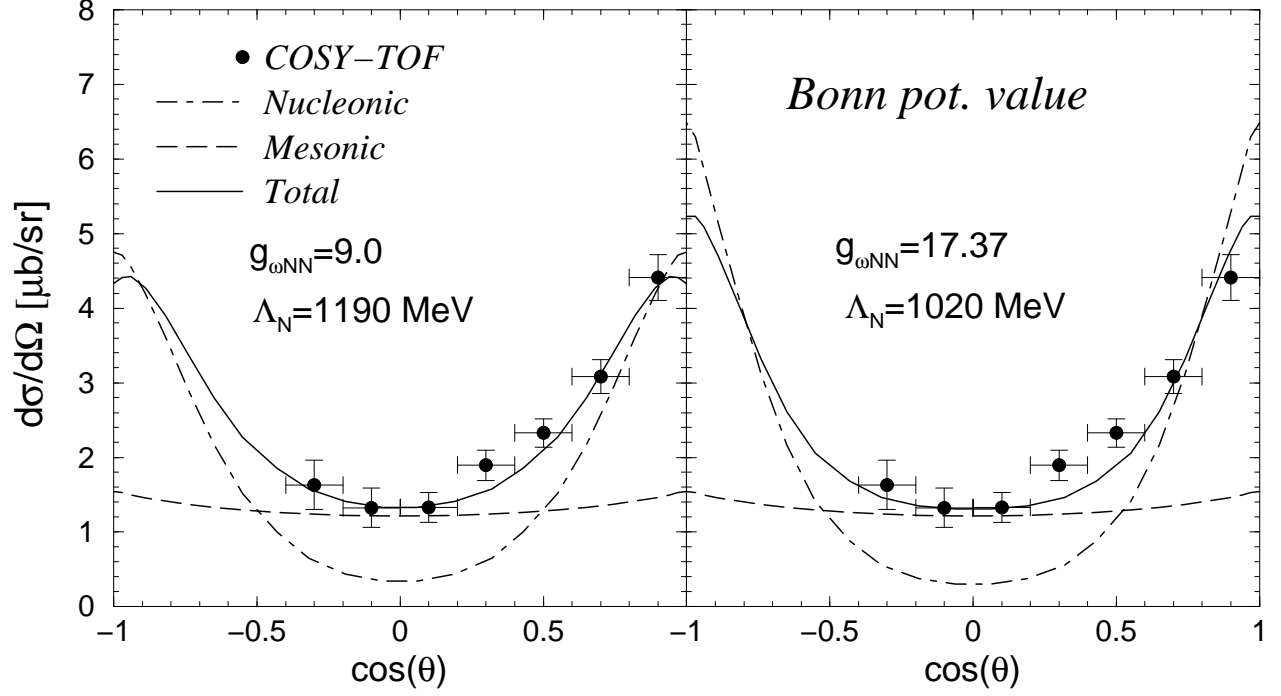


FIG. 4.  $g_{\omega NN}$  dependence of the  $\omega$  angular distribution at excess energy  $Q = 173$  MeV. The left panel is one of the reasonable fits achieved with  $g_{\omega NN} = 9.0$ , while the right panel is the result obtained with the value  $g_{\omega NN} = 17.37$ , which is approximately the value used in the Bonn  $NN$  potential model [41]. Both calculations use the value,  $\kappa_\omega = -2.0$ . Also, see the caption of Fig. 3.

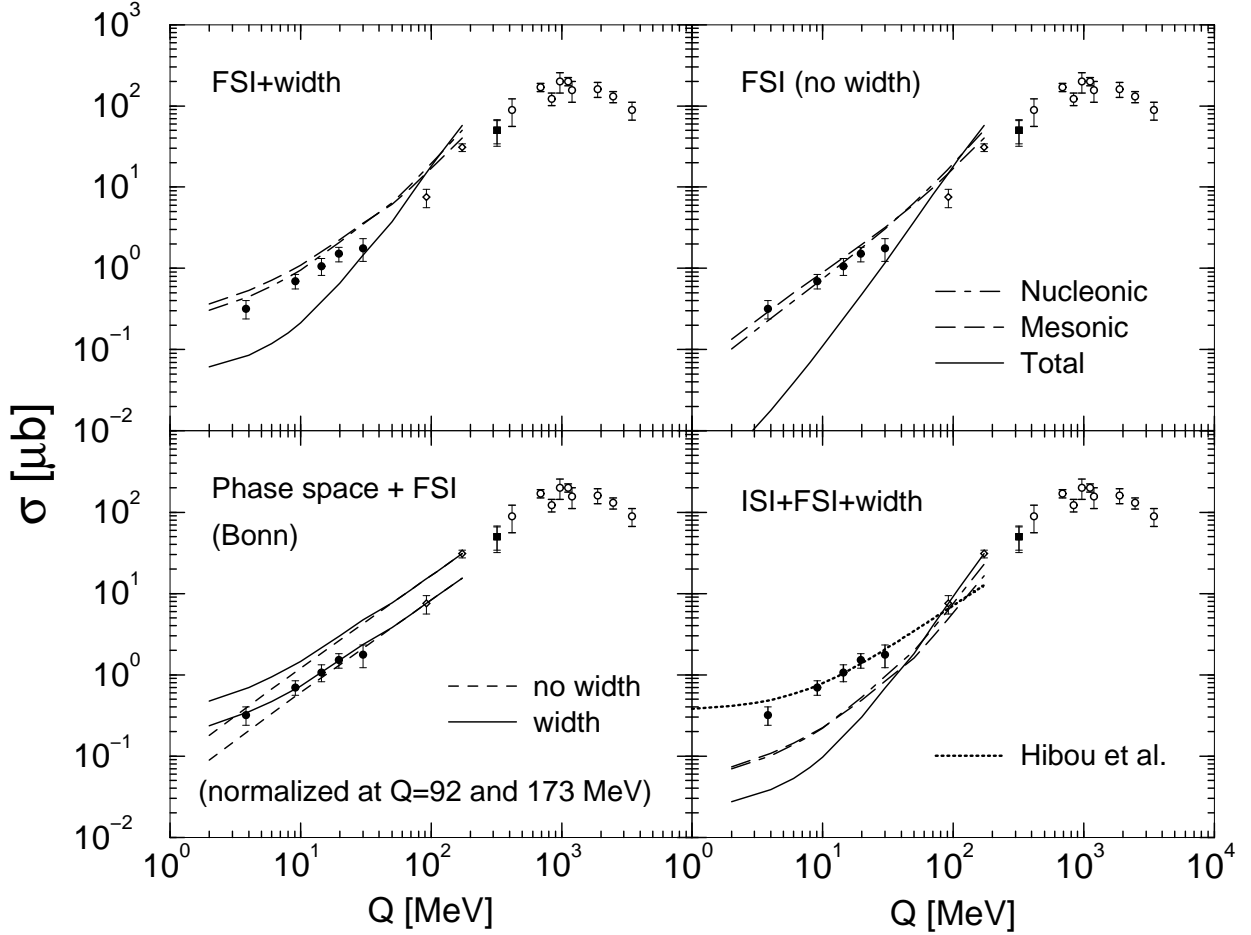


FIG. 5. Energy dependence of the total cross section for the  $pp \rightarrow pp\omega$  reaction without the inclusion of resonances. “ISI”, “FSI” and “width” stand for the  $pp$  initial state interaction,  $pp$  final state interaction, and effects of the  $\omega$  width, respectively. The result with “ISI+FSI+width” (the bottom-right panel) should be compared with the data, where those panels without any of the legends, “ISI”, “FSI” and “width”, imply that the corresponding effect is switched off from the full calculation (the bottom-right panel). Data are from SATURNE [37] (dots), COSY-TOF [38] (diamonds) and Ref. [36] (circles and a filled square), respectively. “Hibou et al.” (the bottom-right panel) stands for the result used in the analysis in Ref. [37]. In the bottom-left panel indicated by “Phase space + FSI”, the calculated energy dependences are normalized to the total cross section data from COSY-TOF [38] at either  $Q = 92$  or  $173$  MeV, where “ $(\epsilon^* \cdot J) = \text{constant}$ ” is used in Eq. (1), and thus, effects of the FSI generated by the Bonn NN potential model [41] enter.

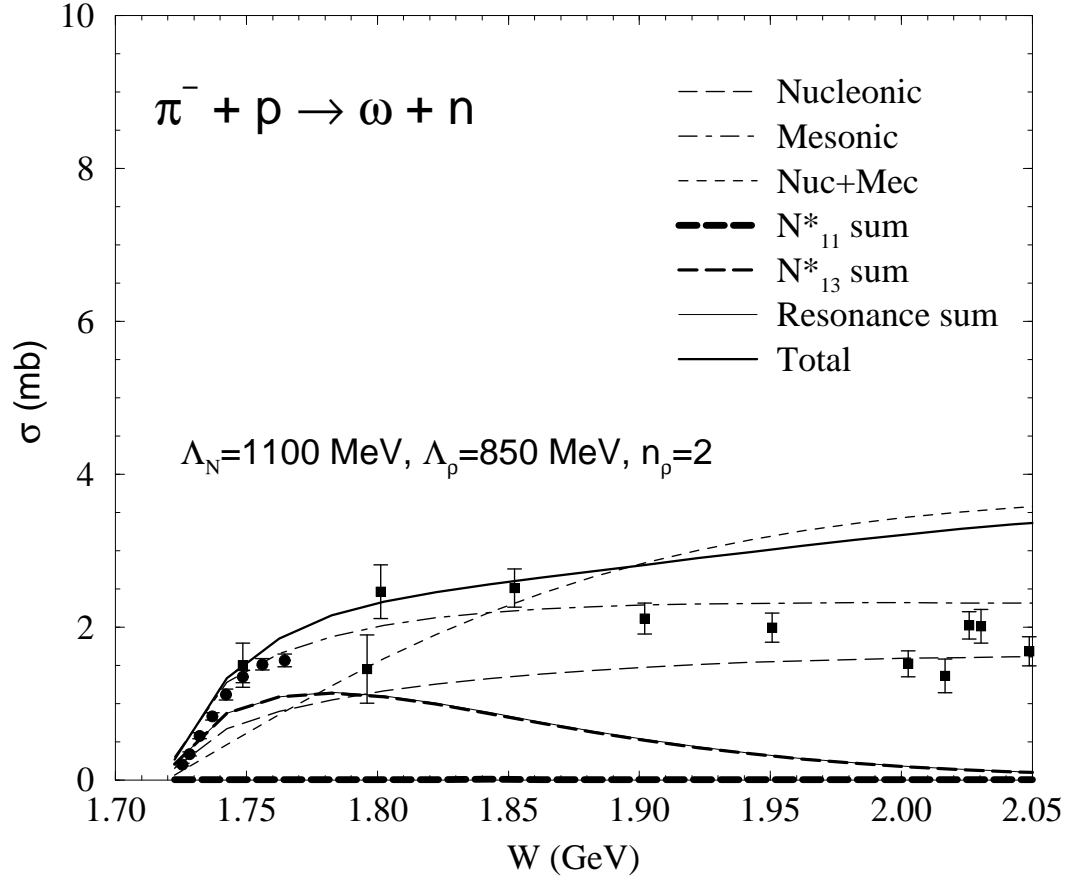


FIG. 6. Energy dependence of the total cross section for the  $\pi^- + p \rightarrow \omega n$  reaction obtained with the preferred model parameter set. Data are from Ref. [60]. Note that at an excess energy of  $Q = 173 \text{ MeV}$  in the  $pp \rightarrow pp\omega$  reaction, the maximum center-of-mass energy  $W$  for this reaction reaches  $\simeq 1.9 \text{ GeV}$ .

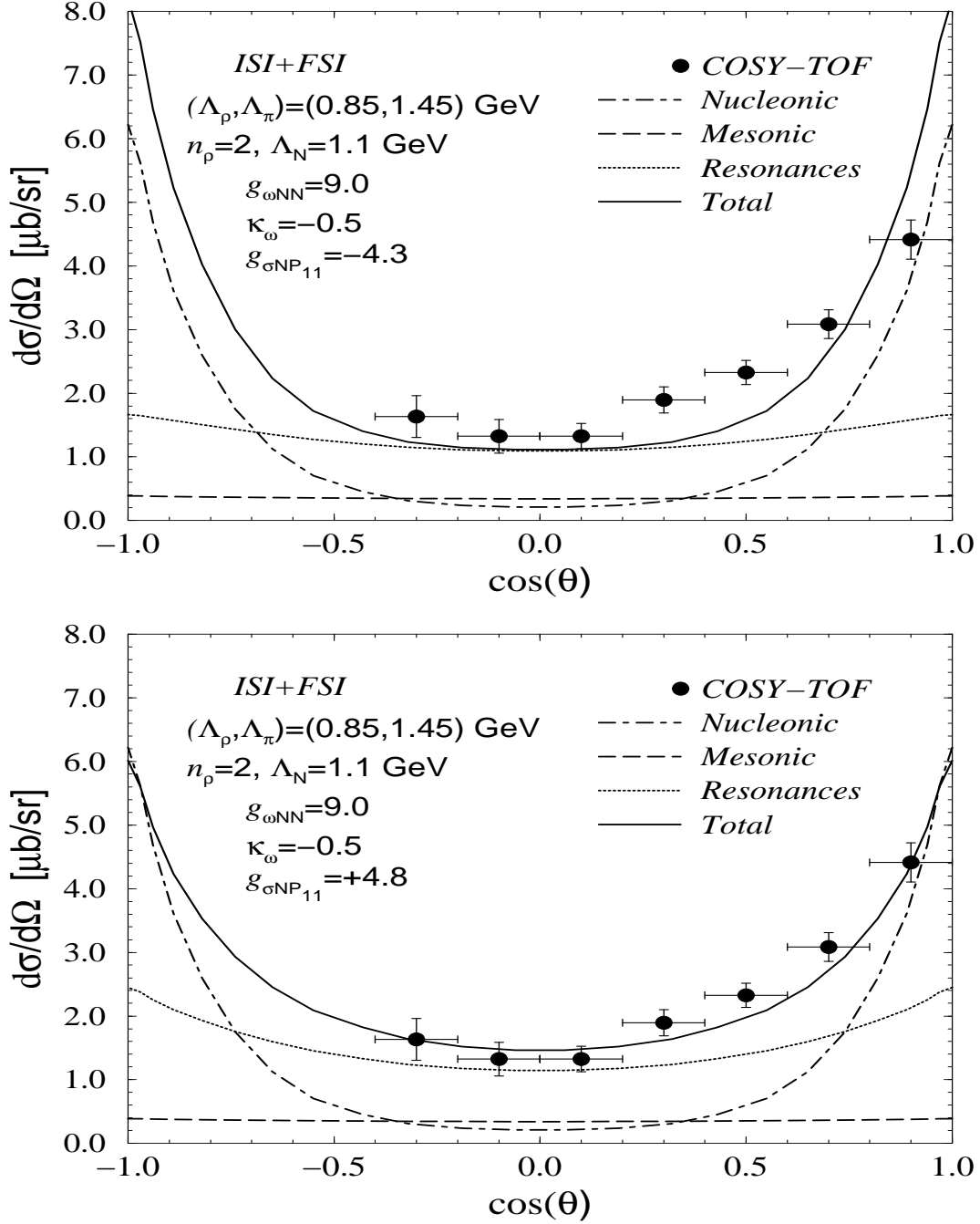


FIG. 7. Calculated  $\omega$  angular distribution for the  $pp \rightarrow pp\omega$  reaction at excess energy  $Q = 173$  MeV. The cut-off parameter  $\Lambda_N$  in the  $\omega NN$  form factor,  $F_N(p^2) = \Lambda_N^4 / [\Lambda_N^4 + (p^2 - m_N^2)]$  [Eq. (11)], is adjusted to the  $\pi^- p \rightarrow \omega n$  reaction  $\Lambda_N = 1100$  MeV (Fig. 6), and the coupling constant  $g_{\sigma NP_{11}}$  is fitted to reproduce the total cross section of  $30.8 \mu\text{b}$  at  $Q = 173$  MeV. The cut-off parameters and  $n_\rho$  indicated in each panel enter at the  $\omega\rho\pi$  vertex form factor:  $F_{\pi\rho\omega}(q_\pi^2, q_\rho^2) \equiv F_\rho(q_\pi^2) \times F_\pi(q_\rho^2) = [\Lambda_\rho^2 / (\Lambda_\rho^2 - q_\rho^2)]^{n_\rho} \times [(\Lambda_\pi^2 - m_\pi^2) / (\Lambda_\pi^2 - q_\pi^2)]$  [Eq. (23)], with  $n_\rho = 2$ ,  $\Lambda_\rho = 850$  MeV and  $\Lambda_\pi = 1450$  MeV, respectively. Also, see the caption of Fig. 3.

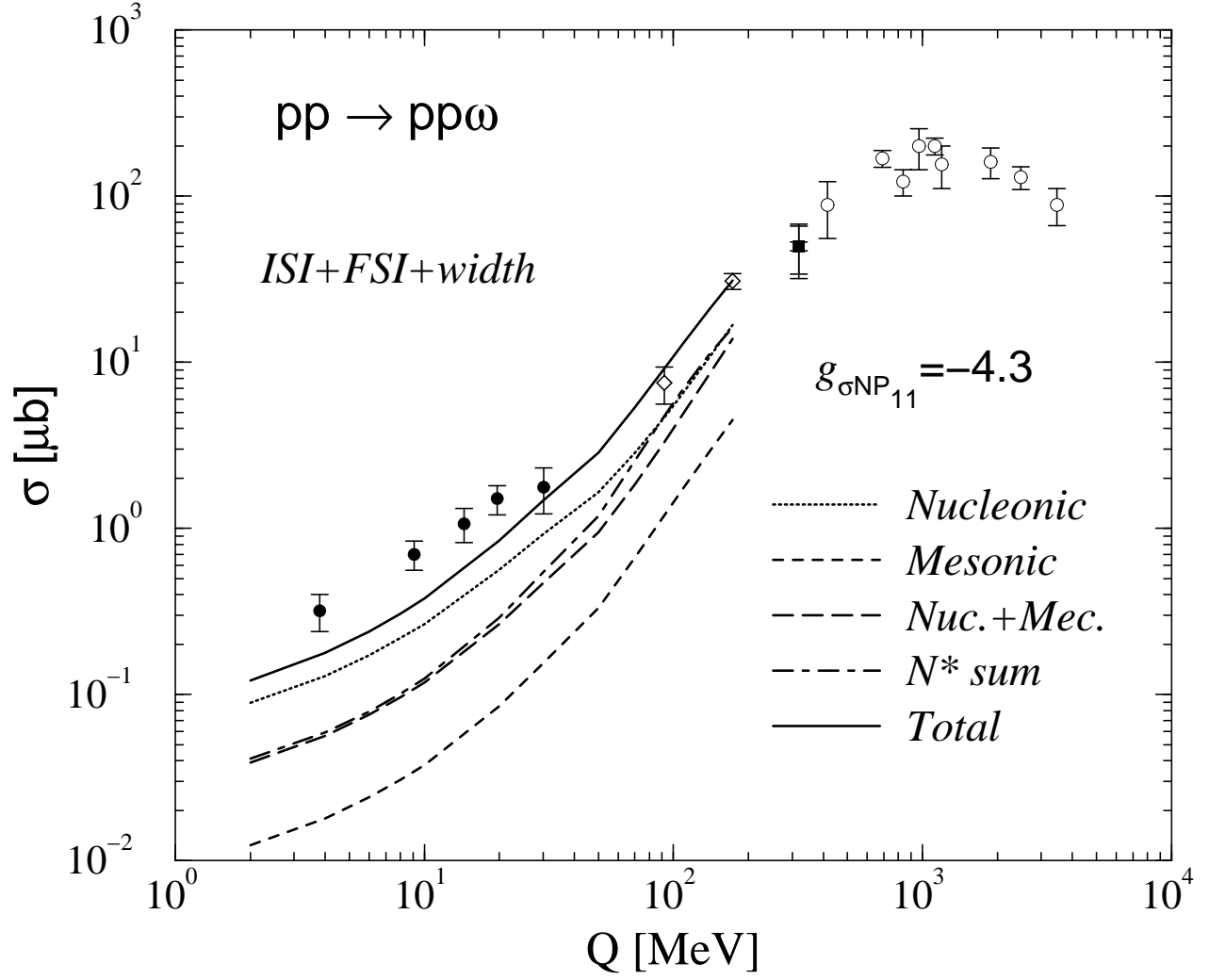


FIG. 8. Calculated energy dependence of the total cross section for the  $pp \rightarrow pp\omega$  reaction with the inclusion of nucleon resonances,  $S_{11}(1535)$ ,  $P_{11}(1710)$ ,  $D_{13}(1700)$  and  $P_{13}(1720)$ . Also, see the caption of Fig. 5.

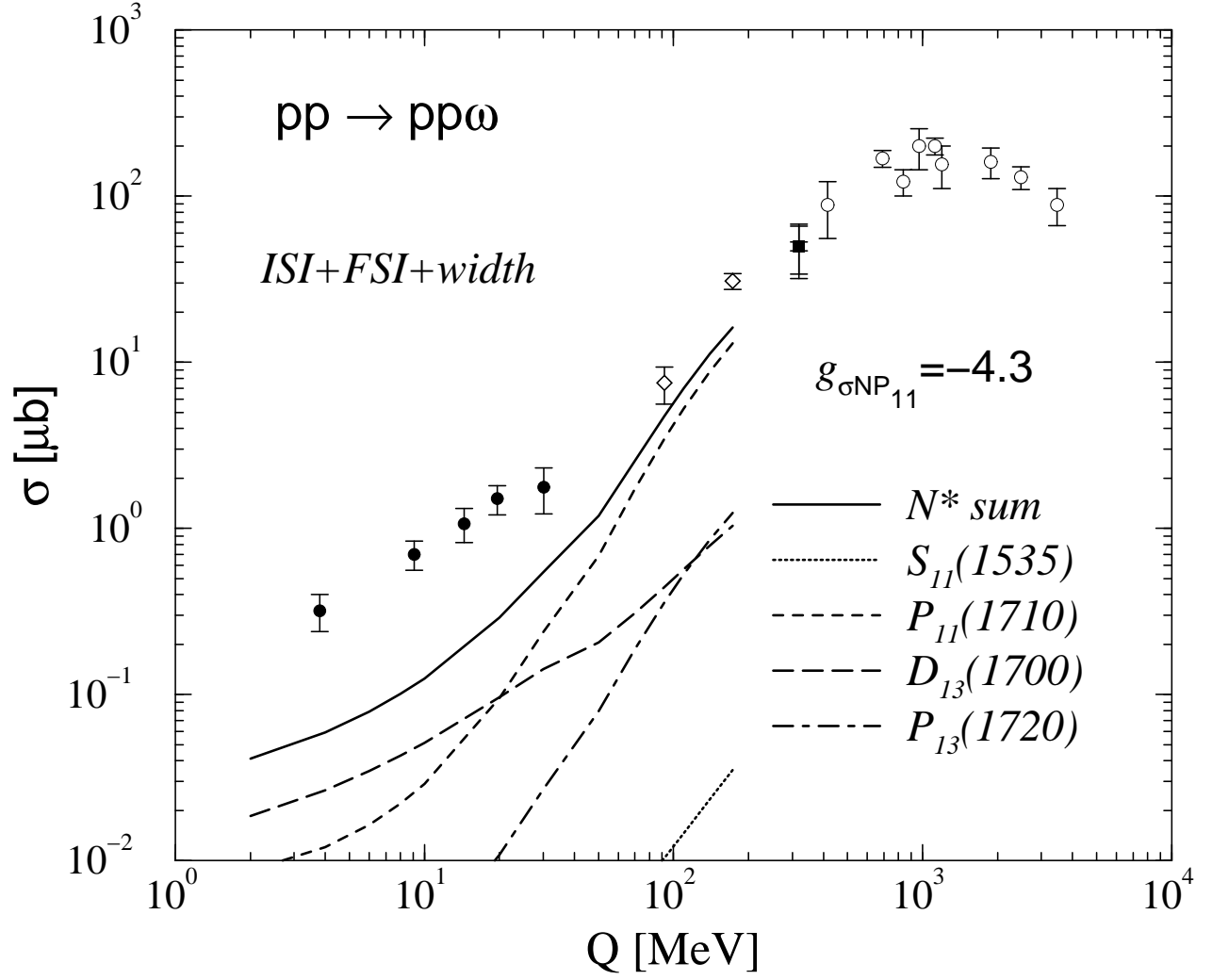


FIG. 9. Decomposition of resonance contributions for the energy dependence of the  $pp \rightarrow pp\omega$  total cross section. Also, see the caption of Fig. 5.



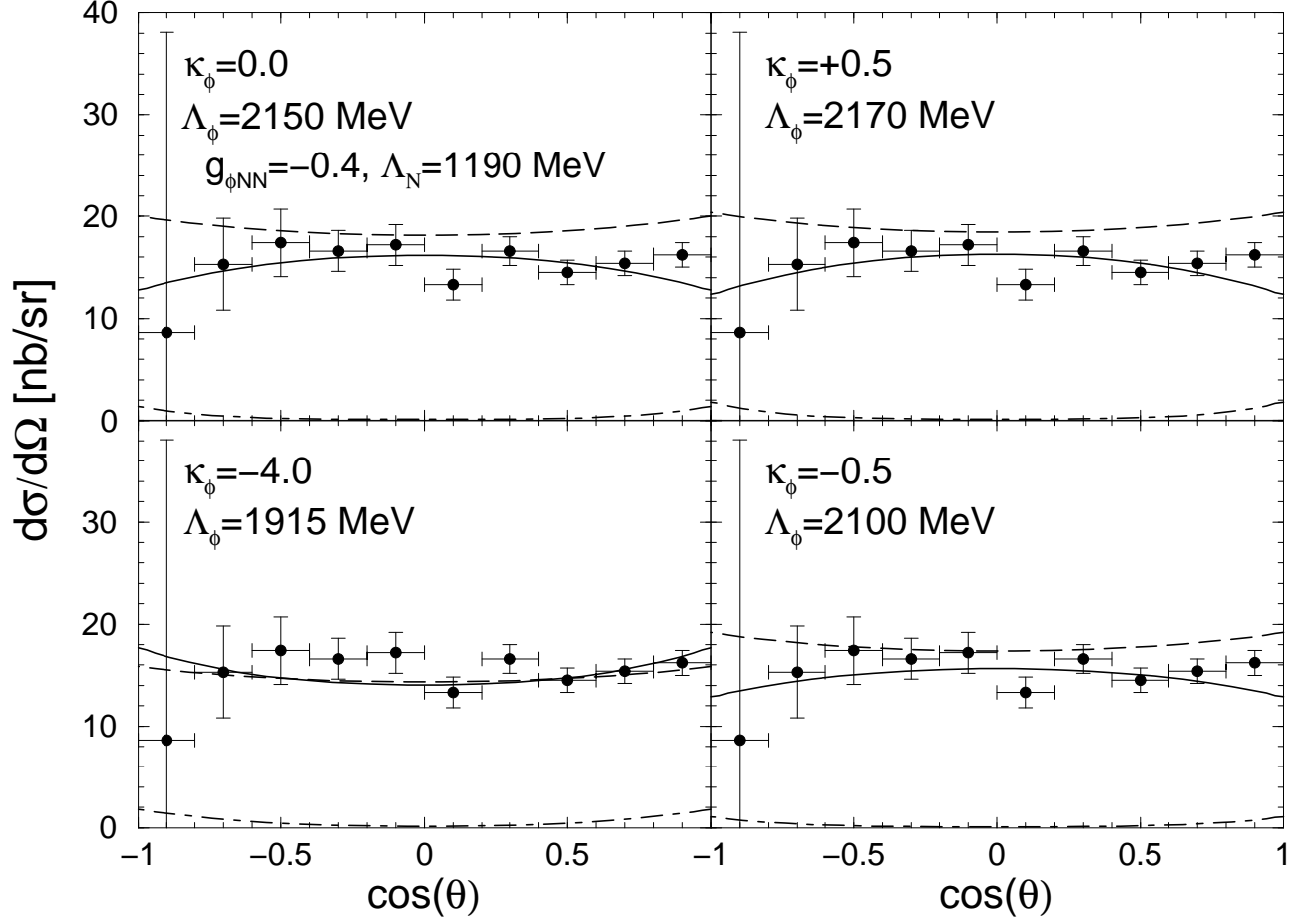


FIG. 10.  $\kappa_\phi$  dependence of the  $\phi$  angular distribution at  $Q = 83$  MeV. The (dashed, dot-dashed, solid) lines show the (mesonic, nucleonic, total) contributions, respectively. The  $\phi NN$  coupling constant and the cut off parameter  $\Lambda_N$  associated with the  $\phi NN$  meson production vertex are fixed at  $g_{\phi NN} = -0.4$  and  $\Lambda_N = 1190$  MeV, and the cut-off parameter  $\Lambda_\phi \equiv \Lambda_\rho = \Lambda_\pi$  in the  $\phi\rho\pi$  meson production vertex is fitted to reproduce the total cross section of  $190\text{nb}$  at  $Q = 83$  MeV. The dots are the data from DISTO [9](a).

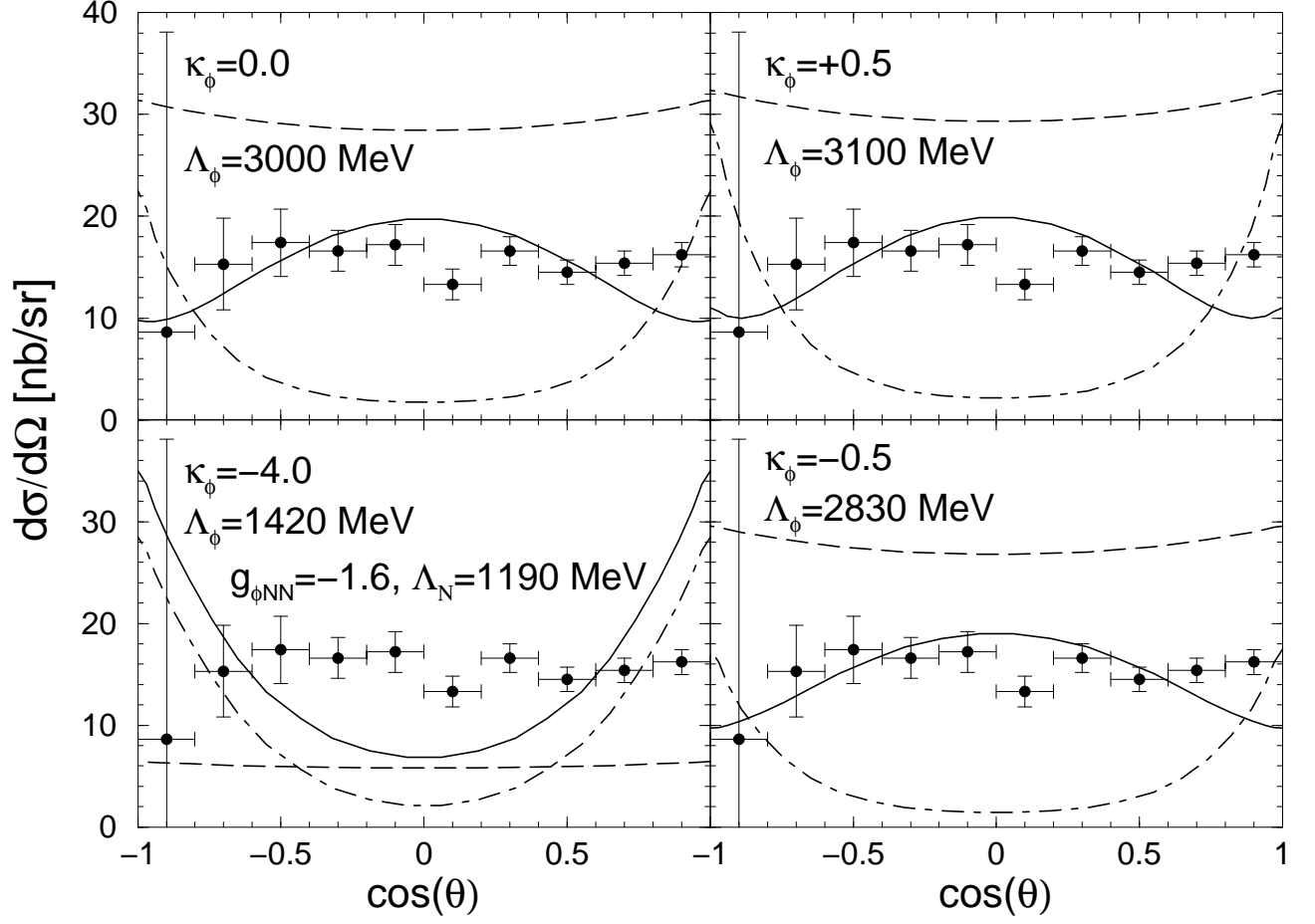


FIG. 11. Same as Fig. 10, but  $g_{\phi NN} = -1.6$ .

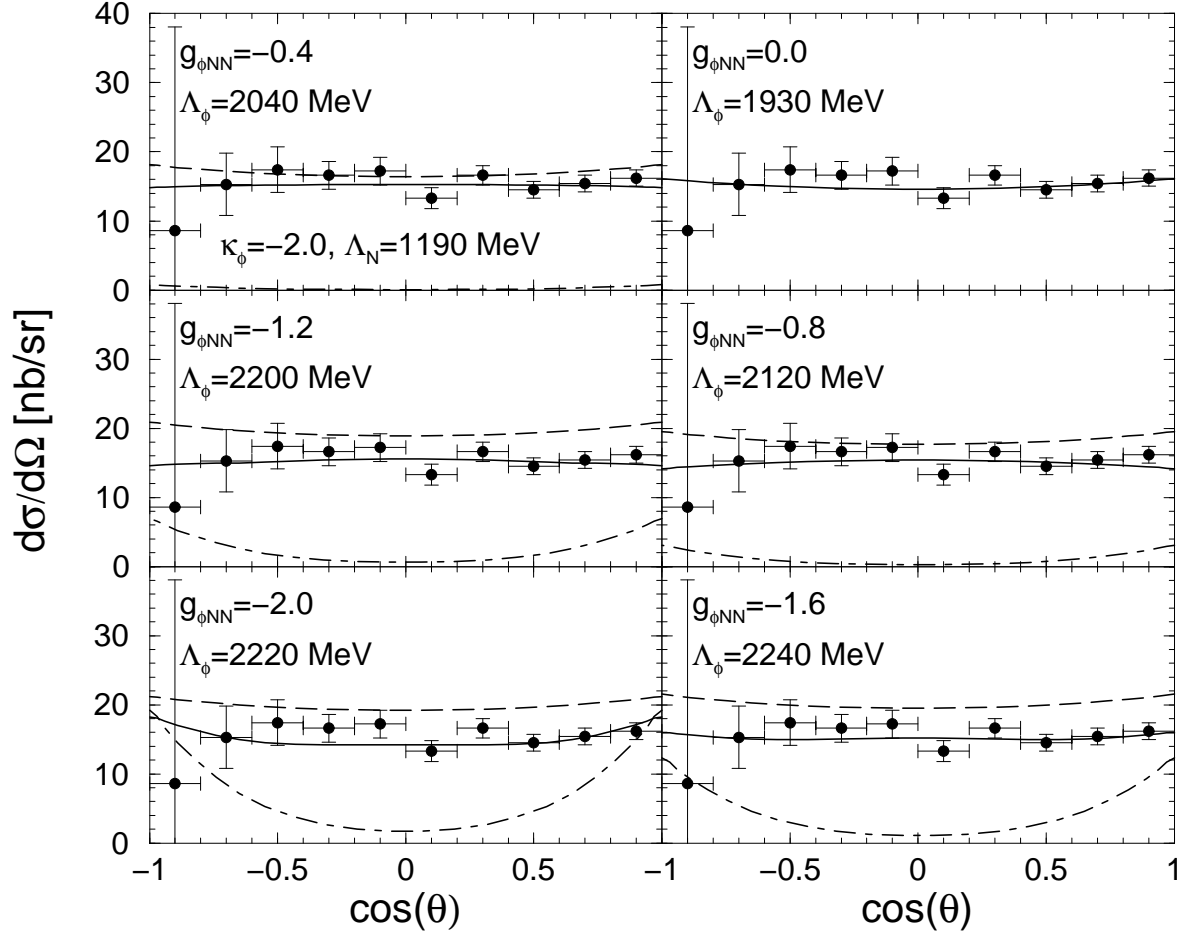


FIG. 12.  $g_{\phi NN}$  dependence of the  $\phi$  angular distribution with the fixed value  $\kappa_\phi = -2.0$ , and  $\Lambda_N = 1190$  MeV. Also, see the caption of Fig. 10.

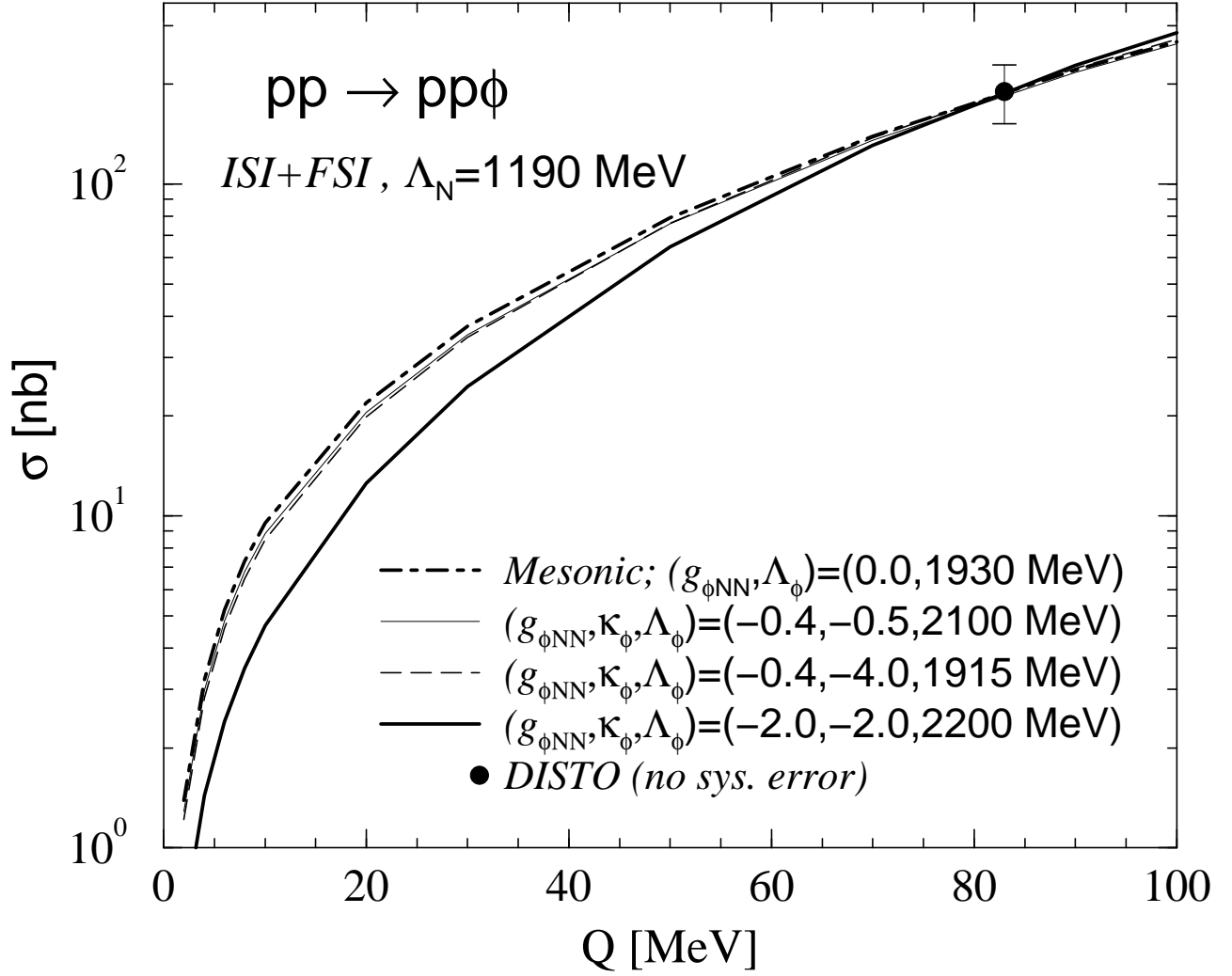


FIG. 13. Energy dependence of the total cross section for the  $pp \rightarrow pp\phi$  reaction, calculated using the four parameter sets, which can reproduce the  $\phi$  angular distribution data [9]. A systematic error in the data point from DISTO [9] is not included.